Super-Resolution of Positive Sources:
the Discrete Setup

Veniamin I. Morgenshtern[1] and Emmanuel J. Candès[1,2]

[1]Dept. of Statistics, Stanford University, CA
[2]Dept. of Mathematics, Stanford University, CA

April 6, 2015

Abstract

In single-molecule microscopy it is necessary to locate with high precision point sources from noisy observations of the spectrum of the signal at frequencies capped by f_c, which is just about the frequency of natural light. This paper rigorously establishes that this super-resolution problem can be solved via linear programming in a stable manner. We prove that the quality of the reconstruction crucially depends on the Rayleigh regularity of the support of the signal; that is, on the maximum number of sources that can occur within a square of side length about $1/f_c$. The theoretical performance guarantee is complemented with a converse result showing that our simple convex program convex is nearly optimal. Finally, numerical experiments illustrate our methods.

1 Introduction

The problem of super-resolution arises in many areas of science and engineering including mass-spectrometry, radar imaging, and wireless communication. In optics, for example, the natural resolution of microscopes is inversely proportional to the wavelength of light used for observation. This happens because of the diffraction of light, and makes it fundamentally difficult to study sub-wavelength features of the object; e.g. to resolve nearby sources located at distances smaller than the diffraction limit. This paper is about this problem: namely, the super-resolution of positive sources, e.g. fluorescing molecules as in single-molecule imaging.

Formally, consider a high-frequency signal

$$x(\mathbf{w}) = \sum_i x_i \delta(\mathbf{w} - \mathbf{w}_i) \tag{1}$$

consisting of positive point sources located at unknown positions $\mathbf{w}_i$ and of unknown intensity $x_i > 0$. The signal is observed through a convolution of the form

$$s(\mathbf{v}) = \int f_{\text{low}}(\mathbf{v} - \mathbf{w}) x(\mathbf{w}) d\mathbf{w} + z(\mathbf{v}), \tag{2}$$

where $f_{\text{low}}(\cdot)$ is a low-frequency kernel that erases the high-frequency components of the signal and $z(\cdot)$ is noise. The goal of super-resolution is to accurately estimate $x(\cdot)$, i.e., the source locations and intensities.

1.1 Super-resolution microscopy

Since our mathematical models and theoretical results are motivated by very concrete contemporary problems in single-molecule imaging, we find it best to pause and introduce some background material; for details beyond those we provide below, please check the wonderful book by J. Goodman [1].
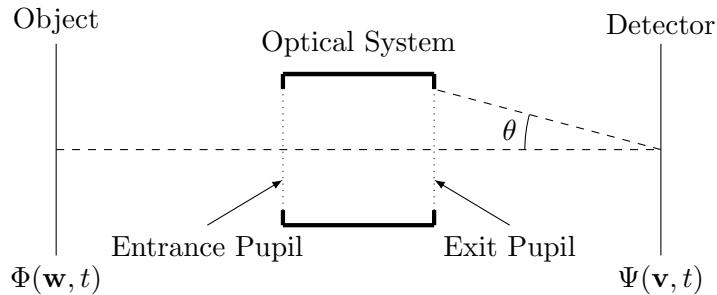

Figure 1: Model of an optical system.

To understand where (2) comes from, we derive the input-output relation of a simple imaging system as shown in Figure 1. While the laws of optics are governed by Maxwell's equations, which are linear, the vectorial nature of the electric and magnetic fields can be neglected in Fourier optics and the physics fully described via the time-varying phasor [1, Sec. 3.2], a term assigned to any of the three components of these two fields. Assume that a narrow-band (not necessarily monochromatic) light is used for illumination, and let $\Phi(\mathbf{w}, t)$ and $\Psi(\mathbf{v}, t)$ respectively denote the input/output phasors describing the field emitted by the object being imaged and the field generated at the receiver of the system. Here, $\mathbf{w}, \mathbf{v} \in \mathbb{R}^2$ are indexing spatial coordinates in the object plane and in the detector plane, respectively, and $t \in \mathbb{R}$ is indexing time. We assume, for convenience, that the phasors $\Phi(\mathbf{w}, t), \Psi(\mathbf{v}, t)$ have been frequency-shifted (as a function of t) to be centered around the mean frequency of the optical wave [1, p. 132], so that, for example, $E(\mathbf{w}, t) = \Re[\Phi(\mathbf{w}, t)e^{2\pi i \bar{\nu} t}]$, where E is one of the components of the electric field and $\bar{\nu}$ is the average frequency of emitted light. The diffraction of light in the optical system can be described by the Fraunhofer approximation leading to [1, Eq (6-6)]

$$\Psi(\mathbf{v}, t) = \int h(\mathbf{v} - \mathbf{w})\Phi(\mathbf{w}, t)d\mathbf{w}, \tag{3}$$

where $h(\mathbf{v})$ is the point-spread function (PSF) of the optical system. In general, the Fourier transform of $h(\cdot)$ is proportional to the indicator function of the aperture and because the aperture is finite, $h(\cdot)$ is band-limited. To be concrete, assume that the entrance and the exit pupils in Figure 1 are square. In this case [1, Sec. 6.2.2]

$$h(\mathbf{v}) \propto \frac{1}{\sqrt{2\bar{f}_c}} \frac{\sin(2\pi \bar{f}_c v_1)}{\pi v_1} \frac{1}{\sqrt{2\bar{f}_c}} \frac{\sin(2\pi \bar{f}_c v_2)}{\pi v_2}, \quad \mathbf{v} = [v_1, v_2]^\mathsf{T}. \tag{4}$$

The spatial frequency cut-off of the optical system is given by

$$\bar{f}_c = \frac{\sin(\theta)}{\lambda},$$

where λ is the wavelength of emitted light (average wavelength in the narrow-band illumination case) and θ is half of the angle spanned by the exit pupil as seen from the center of the image plane

(see Figure 1). Note that due to the narrow-band illumination assumption, $h(\cdot)$ depends upon the average wavelength of the optical wave, but not upon the specific frequencies in the illuminating spectrum so that the system model is described by the simple convolution equation (3).

In optics, the carrier frequency $\bar{\nu} \sim 500\,\text{THz}$ is much higher than the frequency $f_{\text{HET}} \sim 10\,\text{GHz}$, which electronic components can respond to, e. g. the frequency of heterodyne used to down-convert the signal. Consequently, in optics only the time-average of the instantaneous intensity of received light (called received intensity) is directly observable [1, Eq (6-8)]:

$$\tilde{s}(\mathbf{v}) \triangleq \langle \Psi(\mathbf{v}, t)\Psi^*(\mathbf{v}, t) \rangle, \tag{5}$$

where $\Psi^*(\cdot)$ denotes the complex conjugate of $\Psi(\cdot)$ and $\langle \cdot \rangle$ stands for time averaging:

$$\langle g(t) \rangle = f_{\text{HET}} \int_0^{1/f_{\text{HET}}} g(t)dt.$$

In a majority of microscopy applications, the object emits incoherent light. Mathematically, this situation is described by assuming that frequencies of spatially separated emitters vary in statistically independent fashions. This idealized property may be represented by the equation [1, Eq (6-14)]

$$\left\langle \Phi(\mathbf{w}, t)\Phi^*(\mathbf{w}', t) \right\rangle = \delta(\mathbf{w} - \mathbf{w}')x(\mathbf{w}). \tag{6}$$

The quantity $x(\mathbf{w})$ is the time-average of the instantaneous intensity of light emitted by the object and is called *emitted intensity*. Substituting (3) into (5) and then using (6) we obtain the following input-output relation

$$\tilde{s}(\mathbf{v}) = \int f_{\text{low}}(\mathbf{v} - \mathbf{w})x(\mathbf{w})d\mathbf{w}, \quad f_{\text{low}}(\mathbf{v} - \mathbf{w}) \triangleq |h(\mathbf{v} - \mathbf{w})|^2. \tag{7}$$

Observe that (7) is a linear convolution equation with respect to emitted intensity; compare to (3), which is a linear convolution equation with respect to the components of the emitted field. The low-frequency kernel $f_{\text{low}}(\cdot)$ is the square of the two-dimensional (2D) sinc kernel (4) and has a spatial frequency cut-off at $f_c = 2\bar{f}_c$ (twice that of the kernel $h(\cdot)$). The emitted intensity $x(\cdot)$ is a nonnegative function, a property that is crucially important for all results in this paper. Finally, the ℓ_1 norm of the signal,

$$\|x(\cdot)\|_1 = \int |x(\mathbf{w})|d\mathbf{w},$$

has the meaning of cumulative emitted intensity or total energy of light emitted per second. As a side remark, note that when the sample is illuminated by coherent light, as in X-ray crystallography, the resulting input-output relations is no longer linear, in stark contrast to (7), and the phase retrieval problem needs to be solved. For the interested reader, this point is explained in Appendix B.

Our goal is to reconstruct the signal $x(\cdot)$ from the observations $\tilde{s}(\cdot)$ in (7). Without additional structural assumptions on $x(\cdot)$, this is clearly not possible, because the high-frequency components of $x(\cdot)$ are lost. The details of $x(\cdot)$ that are smaller than the Rayleigh diffraction limit,[1] $1.22/\bar{f}_c$, cannot be distinguished [1, Sec 6.5.2]. In single-molecule microscopy [2–4], a modern imaging technique, the signal $x(\cdot)$ consists of several disjoint molecules emitting light. Here, the size of each molecule is about $4\,\text{nm}$, which is much smaller than $1/\bar{f}_c \approx 200\,\text{nm}$, and yet it is absolutely

---

[1]The specific value of the constant, 1.22, is largely a historical convention; the point here is that the details of the image that are much smaller than $1/\bar{f}_c$ are blurred.

necessary to estimate the locations of these molecules with precision that is significantly higher than the Rayleigh diffraction limit.

The main contribution of this paper is to show that under the structural model (1), it is possible to estimate $x(\mathbf{w})$ via linear programming stably from noisy data—all imaging systems are fundamentally noisy—with resolution beyond the diffraction limit. Further, the quality of estimation fundamentally depends on how regularly (in the sense explained in Section 2) the sources/molecules are distributed in the image domain.

1.2 Mathematical models and methods

The super-resolution theory developed in this paper is discrete, which means that the input signal $x(\cdot)$ is assumed to be supported on a fine grid. The nonzero elements of this discrete signal are suggestively called "spikes". In optics, there is no grid, of course; the spikes in (1) can be in arbitrary (continuous) locations, and the companion paper [5] shows how to generalize our key result to the continuous setting. In truth, the analysis of the continuous-space problem is far more technical than that presented here; however, the final result—the stability estimate in (18)—is essentially the same. For now, the advantage of working with a discrete model is that we can explain the key concepts without bothering with heavy mathematical machinery.

1.2.1 Discrete setup

A noiseless discrete model is of the form

$$\tilde{\mathbf{s}} = \mathbf{Q}\mathbf{x}, \tag{8}$$

where $\mathbf{x}$ is either a one- or two-dimensional discrete array of intensities, $\mathbf{Q}$ models the (discrete) convolution equation and $\tilde{\mathbf{s}}$ is the output data, assumed to be of the same dimension(s) as the input vector $\mathbf{x}$. We have already seen examples of PSFs or convolutions; for instance, $f_{\text{low}}(\cdot)$ in (7) is the square of the sinc kernel (in each direction), the sinc kernel being an ideal low-pass filter whose frequency response is a box function. Therefore, the frequency response of $f_{\text{low}}(\cdot)$ is a triangle function in 1D and a pyramid in 2D. In (10), (12), (16) and (17) below, we consider natural PSFs in one and two dimensions so that in the remainder, $\mathbf{Q}$ in (8) or (9) may be given by any of these.

1.2.2 Noise

In modern microscopy applications, the intensities of emitted/received light are very low and in such regimes, the main source of noise is due to quantum-mechanical effects. We have argued that a component of $\tilde{\mathbf{s}}$ represents the expected number of photons to be recorded per unit time at a given pixel on the detector. The actual number of photons detected may be modeled as a Poisson-distributed random variable so that $\mathbf{s} \sim \text{Pois}(\tilde{\mathbf{s}})$, meaning that we have independent Poisson variables with means given by (8). In this paper, we shall work with a slightly more general signal-dependent additive noise $\mathbf{z} = \mathbf{s} - \mathbf{Q}\mathbf{x}$ so that the input-output (IO) relation becomes

$$\mathbf{s} = \mathbf{Q}\mathbf{x} + \mathbf{z}. \tag{9}$$

1.2.3 Recovery

Our recovery method from the observations $\mathbf{s}$ in (9) is extremely simple: solve

$$\min_{\hat{\mathbf{x}}} \quad \|\mathbf{s} - \mathbf{Q}\hat{\mathbf{x}}\|_1 \quad \text{s.t.} \quad \hat{\mathbf{x}} \geq \mathbf{0}. \tag{CVX}$$

In other words, we are looking for a superposition of positive sources such that the mismatch in received intensities is minimum. Note that this method does not make any assumption about the signal and does not make use of any knowledge other than the received data $\mathbf{s}$ and the PSF $\mathbf{Q}$. Furthermore, (CVX) is a simple convex optimization program, which can be recast as a linear program since both $\mathbf{s}$ and $\mathbf{Q}$ are real valued.

1.2.4 Examples of PSFs

We now discuss various models for the discrete convolution equation (9).

1D model with flat spectrum. In our first example, $\mathbf{x} = [x_0 \cdots x_{N-1}]^{\mathsf{T}} \in \mathbb{R}^N$ is a one-dimensional array, and $\mathbf{Q}$ is an ideal low-pass filter in the sense that it has a flat spectrum with a sharp cut-off at f_c. Formally,

$$\mathbf{Q} = \mathbf{Q}_{\text{flat,1D}} = \mathbf{F}^{\mathsf{H}} \hat{\mathbf{Q}}_{\text{flat,1D}} \mathbf{F}, \tag{10}$$

where

$$[\mathbf{F}]_{k,l} = \frac{1}{\sqrt{N}} e^{-\mathrm{i}2\pi kl/N}, \quad -N/2 + 1 \le k \le N/2, \ 0 \le l \le N - 1,$$

is the $N \times N$ discrete Fourier transform (DFT) and $\hat{\mathbf{Q}}_{\text{flat,1D}} = \text{diag}([\hat{p}_{-N/2+1} \cdots \hat{p}_{N/2}]^{\mathsf{T}})$ with

$$\hat{p}_k = \begin{cases} 1, & k = -f_c, \ldots, f_c, \\ 0, & \text{otherwise.} \end{cases} \tag{11}$$

The wavelength $\lambda_c \triangleq 1/f_c$ gives the width of the convolution kernel represented by $\mathbf{Q}$. We assume throughout the paper that N is even for simplicity.

1D model with triangular spectrum. The discrete one-dimensional analog of our imaging system with incoherent light (7) is given by (8), where $\mathbf{Q}$ is as follows:

$$\mathbf{Q} = \mathbf{Q}_{\text{tri,1D}} = \mathbf{F}^{\mathsf{H}} \hat{\mathbf{Q}}_{\text{tri,1D}} \mathbf{F}, \tag{12}$$

$\hat{\mathbf{Q}}_{\text{tri,1D}} = \text{diag}(\hat{\mathbf{q}})$ with $\hat{\mathbf{q}} = [\hat{q}_{-N/2+1} \cdots \hat{q}_{N/2}]^{\mathsf{T}}$ and

$$\hat{q}_k = \begin{cases} 1 - \frac{|k|}{f_c + 1}, & k = -f_c, \ldots, f_c \\ 0, & \text{otherwise.} \end{cases} \tag{13}$$

In this model, the nonzero elements of $\mathbf{x}$ represent the molecules at the corresponding locations (on the grid) whereas the components of $\tilde{\mathbf{s}}$ represent the intensity of light measured at the corresponding pixel on the detector.

2D model with flat spectrum. Similarly, the 2D model with a flat spectrum reads

$$\tilde{\mathbf{s}}_{\text{2D}} = \mathbf{F}_{\text{2D}}^{\mathsf{H}} \hat{\mathbf{Q}}_{\text{2D}} \mathbf{F}_{\text{2D}} \mathbf{x}_{\text{2D}}, \tag{14}$$

where $\mathbf{F}_{\text{2D}} : \mathbb{C}^N \times \mathbb{C}^N \to \mathbb{C}^N \times \mathbb{C}^N$ is the linear operator that implements the 2D Fourier transform and acts according to

$$[\mathbf{F}_{\text{2D}} \mathbf{x}_{\text{2D}}]_{k_1,k_2} = \frac{1}{N} \sum_{l_1=0}^{N-1} \sum_{l_2=0}^{N-1} x_{l_1,l_2} e^{-\mathrm{i}2\pi(k_1 l_1 + k_2 l_2)/N}$$

and $\hat{\mathbf{Q}}_{2\mathrm{D}} : \mathbb{C}^N \times \mathbb{C}^N \to \mathbb{C}^N \times \mathbb{C}^N$ is the diagonal operator in the Fourier domain,

$$[\hat{\mathbf{Q}}_{2\mathrm{D}}\mathbf{y}_{2\mathrm{D}}]_{k_1,k_2} = \hat{p}_{k_1-N/2}\hat{p}_{k_2-N/2} \, [\mathbf{y}_{2\mathrm{D}}]_{k_1,k_2}. \tag{15}$$

To keep the same notation, define $\mathbf{x} = \mathrm{vec}(\mathbf{x}_{2\mathrm{D}})$ and $\tilde{\mathbf{s}} = \mathrm{vec}(\tilde{\mathbf{s}}_{2\mathrm{D}})$, where the $\mathrm{vec}(\cdot)$ operation stacks the columns of a matrix into a tall vector. Using the properties of the Kronecker product, (14) can be written as (8) with

$$\mathbf{Q} = \mathbf{Q}_{\mathrm{flat,2D}} = (\mathbf{F}^\mathsf{H} \otimes \mathbf{F}^\mathsf{H})(\hat{\mathbf{Q}}_{\mathrm{flat,1D}} \otimes \hat{\mathbf{Q}}_{\mathrm{flat,1D}})(\mathbf{F} \otimes \mathbf{F}). \tag{16}$$

2D model with triangular spectrum. With the vectorized notation, the 2D model with triangular spectrum can be written as (8) with

$$\mathbf{Q} = \mathbf{Q}_{\mathrm{tri,2D}} = (\mathbf{F}^\mathsf{H} \otimes \mathbf{F}^\mathsf{H})(\hat{\mathbf{Q}}_{\mathrm{tri,1D}} \otimes \hat{\mathbf{Q}}_{\mathrm{tri,1D}})(\mathbf{F} \otimes \mathbf{F}). \tag{17}$$

1.2.5 Intensity normalization

It follows from our earlier discussion that for incoherent light (models with triangular spectra), we may interpret $\|\mathbf{x}\|_1$ as the total intensity of light emitted by the object. Similarly, $\|\tilde{\mathbf{s}}\|_1$ is the total intensity of light observed at the receiver. Letting $[\mathbf{q}_0 \cdots \mathbf{q}_{N-1}]$ denote the columns of $\mathbf{Q}$, (13) guarantees that $\|\mathbf{q}_l\|_1 = 1$ for all l. To see this, first note that $\mathbf{q}_l$ is a shifted version of $\frac{1}{\sqrt{N}}\mathbf{F}^\mathsf{H}\hat{\mathbf{q}}$ so that $\|\mathbf{q}_l\|_1 = \|\frac{1}{\sqrt{N}}\mathbf{F}^\mathsf{H}\hat{\mathbf{q}}\|_1$. Next, write $\hat{\mathbf{q}} = \hat{\mathbf{d}} \star \hat{\mathbf{d}}$ where $\hat{\mathbf{d}} = [\hat{d}_{-N/2+1} \cdots \hat{d}_{N/2}]^\mathsf{T}$ and

$$\hat{d}_k = \begin{cases} \sqrt{\frac{1}{f_c+1}}, & k = -f_c/2, \ldots, f_c/2, \\ 0, & \text{otherwise}, \end{cases}$$

and $\star$ denotes the discrete convolution. Finally, use the convolution theorem to conclude

$$\|\mathbf{q}_l\|_1 = \left\| \frac{1}{\sqrt{N}}\mathbf{F}^\mathsf{H}\hat{\mathbf{q}} \right\|_1 = \left\| \frac{1}{\sqrt{N}}\mathbf{F}^\mathsf{H}(\hat{\mathbf{d}} \star \hat{\mathbf{d}}) \right\|_1 = \left\| \overline{\mathbf{F}^\mathsf{H}\hat{\mathbf{d}}} \odot \mathbf{F}^\mathsf{H}\hat{\mathbf{d}} \right\|_1 = \|\mathbf{F}^\mathsf{H}\hat{\mathbf{d}}\|_2^2 = 1,$$

where $\odot$ denotes the element-wise product and $\bar{\mathbf{a}}$ takes conjugate element-wise. Therefore, using that $x_l \geq 0$ and $\mathbf{q}_l \geq \mathbf{0}$ for all l,

$$\|\tilde{\mathbf{s}}\|_1 = \left\| \sum_{l=0}^{N-1} x_l \mathbf{q}_l \right\|_1 = \sum_{l=0}^{N-1} x_l \|\mathbf{q}_l\|_1 = \sum_{l=0}^{N-1} x_l = \|\mathbf{x}\|_1.$$

Hence, our normalization is such that the intensity of light (emitted energy per second) is conserved in the system. In the models (11) and (15) with a flat spectrum the ℓ_1 norm of the signal is not conserved.

1.3 Notation

Sets are denoted by calligraphic letters $\mathcal{A}, \mathcal{B}$, and so on. Boldface letters $\mathbf{A}, \mathbf{B}, \ldots$ and $\mathbf{a}, \mathbf{b}, \ldots$ denote matrices (or linear operators) and vectors, respectively. The element in the i-th row and j-th column of a matrix $\mathbf{A}$ is a_{ij} or $[\mathbf{A}]_{i,j}$, and the i-th element of the vector $\mathbf{a}$ is a_i or $[\mathbf{a}]_i$. For a vector $\mathbf{a}$, $\mathrm{diag}(\mathbf{a})$ stands for the diagonal matrix that has the entries of $\mathbf{a}$ on its main diagonal. The superscripts $^\mathsf{T}$ and $^\mathsf{H}$ stand for transposition and Hermitian transposition, respectively. For a finite set $\mathcal{I}$, we write $|\mathcal{I}|$ for the cardinality. For two functions $f(\cdot)$ and $g(\cdot)$, the notation $f(\cdot) = \mathcal{O}(g(\cdot))$

means that $\limsup_{t\to\infty} |f(t)/g(t)|$ is bounded. For $x \in \mathbb{R}$, $\lceil x \rceil \triangleq \min\{m \in \mathbb{Z} \mid m \geq x\}$. We use $[l:k]$ to designate the set of natural numbers $\{l, l+1, \ldots, k\}$. The expectation operator is $\mathbb{E}[\cdot]$. For a vector $\mathbf{a} \in \mathbb{C}^n$, $\|\mathbf{a}\|_1 = \sum_{j=0}^{n-1} |a_j|$ and $\|\mathbf{a}\|_2 = \sqrt{\sum_{j=0}^{n-1} |a_j|^2}$ denote the ℓ_1 and ℓ_2 norms, respectively; $\|\mathbf{a}\|$ means either $\|\mathbf{a}\|_1$ or $\|\mathbf{a}\|_2$. The number of nonzero elements of a vector $\mathbf{a}$ is $\|\mathbf{a}\|_0$. For a matrix $\mathbf{A} \in \mathbb{C}^{n\times n}$, the operator norm is defined as $\|\mathbf{A}\|_{1,op} = \max_i \sum_{j=0}^{n-1} |a_{ij}|$ and $\mathrm{vec}(\mathbf{A})$ denotes the n^2-dimensional vector obtained by stacking the columns of $\mathbf{A}$. For vectors $\mathbf{a}$ and $\mathbf{b}$, $\mathbf{a} \odot \mathbf{b}$ denotes the element-wise product; $\mathbf{a} \star \mathbf{b}$ denotes the discrete convolution; the Kronecker product of matrices $\mathbf{A}$ and $\mathbf{B}$ is denoted as $\mathbf{A} \otimes \mathbf{B}$.

2 Main results

Consider the 1D model for concreteness. From (11), (13) we see that we have access to $n = 2f_c + 1$ low-frequency observations while the total number of degrees-of-freedom in $\mathbf{x}$ is N. The ratio $\mathrm{SRF} \triangleq N/n$ is called the *super-resolution factor* (SRF); this is the ratio between $1/n$ and $1/N$, the scale at which we have data and that at which we wish to see details.

As we will review below, the sparsity condition $\|\mathbf{x}\|_0 < n/2$ is sufficient for recovery of $\mathbf{x}$ when there is no noise. If there is noise, it turns out that sparsity is not sufficient as our ability to estimate $\mathbf{x}$ from $\mathbf{s}$ in a stable way fundamentally depends on how regular the positions of the spikes are, i.e., how many spikes may be clustered close together.

2.1 Rayleigh regularity

Suppose we are in D dimensions and think of our discrete signal $\mathbf{x} \in \mathbb{C}^{N^D}$ as samples on the D-dimensional grid $\{0, 1/N, \ldots, 1 - 1/N\}^D \subset \mathbb{T}^D$, where $\mathbb{T}^D$ is the D-dimensional (periodic) torus— the circle in 1D. In this paper, we can think of the ambient dimension D as being either one or two. We introduce a definition of Rayleigh regularity inspired by [6, Def. 1].

Definition 1 (Rayleigh regularity). Fix N, n and set $\lambda_c = 1/f_c = 2/(n-1)$. We say that the set of points $\mathcal{T} \subset \{0, 1/N, \ldots, 1 - 1/N\}^D \subset \mathbb{T}^D$ is Rayleigh regular with parameters (d, r) and write $\mathcal{T} \in \mathcal{R}_D(d, r; N, n)$ if it may be partitioned as $\mathcal{T} = \mathcal{T}_1 \cup \ldots \cup \mathcal{T}_r$ where the $\mathcal{T}_i$'s are disjoint, and each obeys a minimum separation constraint:

1. for all $1 \leq i < j \leq r$, $\mathcal{T}_i \cap \mathcal{T}_j = \emptyset$;

2. for all square subsets $\mathcal{D} \subset \mathbb{T}^D$ of sidelength $d\lambda_c/2$ and all i,
$$|\mathcal{T}_i \cap \mathcal{D}| \leq 1.$$

When no ambiguity arises, we will shortly write $\mathcal{R}_D(d, r)$ instead of $\mathcal{R}_D(d, r; N, n)$.

With a slight abuse of notation, it is also convenient to define a set of Rayleigh regular signals (and nonnegative Rayleigh regular signals) with parameters (d, r):

$$\mathcal{R}_D(d, r) = \{\mathbf{x} \in \mathbb{C}^{N^D} : \mathrm{supp}(\mathbf{x}) \in \mathcal{R}_D(d, r)\},$$
$$\mathcal{R}_D^+(d, r) = \{\mathbf{x} \in \mathbb{R}_+^{N^D} : \mathrm{supp}(\mathbf{x}) \in \mathcal{R}_D(d, r)\},$$

where $\mathrm{supp}(\mathbf{x})$ is the support of $\mathbf{x}$ (the locations on grid where $\mathbf{x}$ does not vanish).

Remark. Intuitively, in 1D, $\mathbf{x} \in \mathcal{R}_1(d, r)$ simply means that the signal $\mathbf{x}$ contains no more than r spikes in any d consecutive Nyquist intervals; a Nyquist interval being of length $\lambda_c/2$, which corresponds to the Nyquist-Shannon sampling rate of a signal that is band-limited to $[-f_c, f_c]$. Figure 2 illustrates these concepts for different parameter values.[2]

We discuss some examples of Rayleigh regular signals and first consider $\mathbf{x} \in \mathcal{R}_1(1, 1)$. This signal may contain one spike per Nyquist interval. Each spike is associated with two unknown parameters: location and amplitude. Since there are n Nyquist intervals, we may have as many as $2n$ unknown parameters in total, which is more than the number n of observations (cf. (13), (11)). Hence, recovery of $\mathbf{x} \in \mathcal{R}_1(1, 1)$ is in general not possible even in the noiseless case. If we however knew the locations of the spikes but not the amplitudes, we could recover the signal $\mathbf{x} \in \mathcal{R}_1(1, 1)$ by solving a system of linear equations.

Next take $\mathbf{x} \in \mathcal{R}_1(2, 1)$. Such a signal may only contain one spike per two Nyquist intervals. Hence, the total number of unknown parameters is at most equal to the number of observations and recovery of $\mathbf{x} \in \mathcal{R}_1(2, 1)$ is barely possible in the noiseless case. For example, as discussed in Section 3, $\mathbf{x}$ can be recovered by Prony's method. In general, $\mathbf{x} \in \mathcal{R}_1(2r, r)$ is the absolute limit for recovery of complex-valued signals in the noiseless case in the sense that $\mathbf{x} \in \mathcal{R}_1(2r - \epsilon, r)$, $\epsilon > 0$, is in general not recoverable.

Strictly speaking, the general dimension-counting considerations above do not hold for positive signals $\mathbf{x} \in \mathbb{R}_+^N$ because the positivity of $\mathbf{x}$ supplies extra information. On the one hand, it is nevertheless possible to construct adversarial signals $\mathbf{x} \in \mathcal{R}_1^+(2r - \epsilon, r)$ that will not be recoverable by any method whatsoever. On the other hand, this paper shows that $\mathbf{x} \in \mathcal{R}_1^+(3.74r, r)$ can be recovered stably in the presence of (small) noise via the linear program (CVX).

2.2 Stable recovery

We are now ready to present our main results; although they extend to higher dimensions, they are stated in 1 and 2D for simplicity. Throughout, we assume that the data $\mathbf{s}$ is given by (9).

Theorem 1 (Flat spectrum). *In 1D, take $\mathbf{Q} = \mathbf{Q}_{\text{flat,1D}}$ and $\mathbf{x} \in \mathcal{R}_1^+(3.74r, r)$ with $f_c \geq 128r$. Then the solution $\hat{\mathbf{x}}$ to (CVX) obeys*

$$\|\hat{\mathbf{x}} - \mathbf{x}\|_1 \leq C \cdot \left(\frac{N}{n-1}\right)^{2r} \cdot \|\mathbf{z}\|_1 \approx C \cdot \text{SRF}^{2r} \cdot \|\mathbf{z}\|_1, \tag{18}$$

where $C = C_1(r)$, only depends on r (if $\text{SRF} \geq 3.03/r$, it can be taken as in (39)).

In 2D, take $\mathbf{Q} = \mathbf{Q}_{\text{flat,2D}}$, $\mathbf{x} \in \mathcal{R}_2^+(4.76r, r)$ with $f_c \geq 512r$. Then (18) holds with a constant C depending on r only, which we do not specify for brevity.

The result in Theorem 1 is not sensitive to the exact choice of the kernel $\mathbf{Q}$ and remains valid for just about any other low-frequency kernel. To illustrate this point and to connect our theory to super-resolution microscopy we now give the result for the PSF discussed in Section 1.1.

Theorem 2 (Triangular spectrum). *Set $1/2 \leq \alpha < 1$. In 1D, take $\mathbf{Q} = \mathbf{Q}_{\text{tri,1D}}$ and assume $\mathbf{x} \in \mathcal{R}_1^+(3.74r/\alpha, r)$ with $f_c \geq 256r$. Then the bound (18) holds with a finite constant $C = C_1(r, \alpha)$, namely,*

$$\|\hat{\mathbf{x}} - \mathbf{x}\|_1 \leq C \cdot \text{SRF}^{2r} \cdot \|\mathbf{z}\|_1. \tag{19}$$

(If $\text{SRF} \geq 3.03/r$, then the constant can be taken as in (41).)

---

[2]Clearly, $\mathcal{R}_1(d, r_1) \subset \mathcal{R}_1(d, r_2)$ for $r_1 \leq r_2$ and $\mathcal{R}_1(d_1, r) \subset \mathcal{R}_1(d_2, r)$ for $d_1 \geq d_2$.
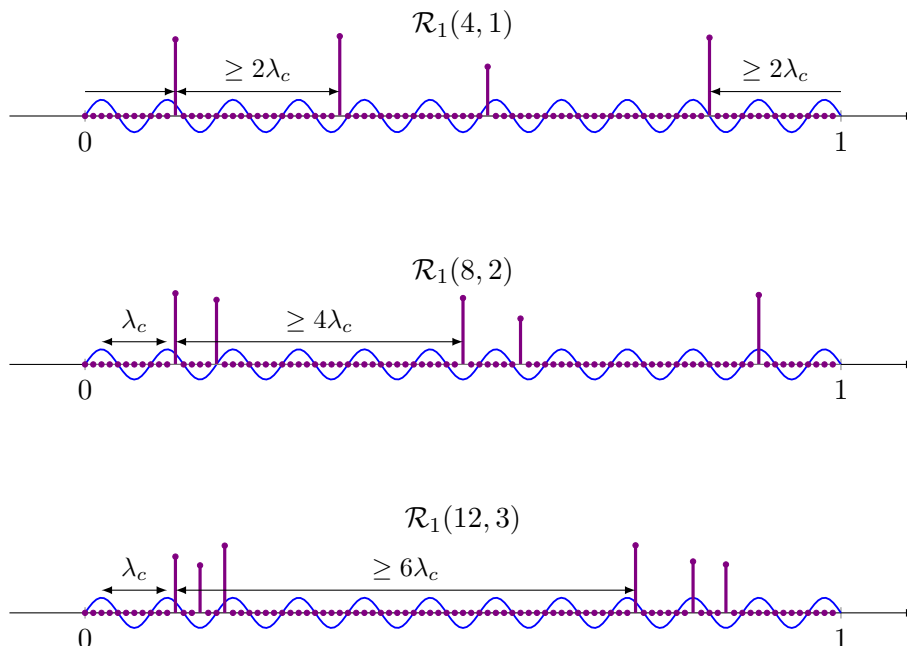
Figure 2: Examples of discrete N dimensional signals from the Rayleigh classes $\mathcal{R}_1(4,1)$, $\mathcal{R}_1(8,2)$, $\mathcal{R}_1(12,3)$ depicted on the grid $\{0, 1/N, \ldots, 1 - 1/N\} \subset \mathbb{T}$. The sine wave $\sin(2\pi f_c t)$ at the highest visible frequency is shown in blue for reference. Here, $N = 92$ and $n = 23$, so that SRF = 4 and $\lambda_c = 1/11$. By periodicity, the endpoints are identified.

In 2D, take $\mathbf{Q} = \mathbf{Q}_{\text{tri,2D}}$, $\mathbf{x} \in \mathcal{R}_2^+(4.76r/\alpha, r)$ with $f_c \geq 1024r$. Then except for the numerical value of the constant, the same conclusion holds.

When $\alpha \to 1$, $C_1(r,\alpha) \to \infty$, which reflects the fact that, as seen from (13), the spectrum of $\mathbf{Q}_{\text{tri,1D}}$ is very small at the border of the interval $[-f_c, f_c]$. Hence, with noise, the spectral components of the signal can only be observed away from this border, for example on the interval $[-0.9f_c, 0.9f_c]$, which corresponds to taking $\alpha = 0.9$ in Theorem 2.

Implications for single-molecule microscopy. Consider Theorem 2 in 2D and remember that $\|\mathbf{z}\|_1$ is the cumulative difference in light intensity between noiseless (ideal) and real observations. Then the theorem tells us that the cumulative error in light intensity in signal estimates is bounded by the amplified version of the cumulative error in light intensity in the data. The noise amplification factor (NAF) behaves as SRF^{2r}, where r is the parameter describing the regularity of the signal support. If the noise level is sufficiently small and the signal is sufficiently regular (r is small), i.e., not too many molecules are clustered close together, and SRF is modest, then the algorithm (CVX) is guaranteed to achieve excellent super-resolution results. As we will explain in Section 2.3, no algorithm can perform substantially better.

Contribution. Theorems 1 and 2 are new, and while their proofs are given in Section 4, we would like to discuss the main technical contribution of this paper. When $r = 1$ or, equivalently, when the spikes are separated by at least $1.87\lambda_c$ and not necessarily positive, a result similar to Theorem 1 was obtained in [7, Th. 1.5] using a different convex program, see also [8] for a continuous-space version; this program, given by (L1) below, requires knowledge of an upper bound on $\|\mathbf{z}\|_1$. The proof in [7]

is based on constructing a (dual) low-frequency trigonometric polynomial that interpolates the sign of the spikes. The crucial observation we make in this paper is that the technique developed in [7] can be extended to the important setting when the spikes are not separated and positive. The proof is based on a simple idea: a Rayleigh-regular set may be partitioned into subsets with points in each subset separated by at least $1.87\lambda_c$; therefore, each set comes with a (dual) low-frequency trigonometric polynomial constructed in [7]; multiplying such polynomials together gives a low-frequency polynomial interpolating the signal.

In the noiseless setting ($\mathbf{z} = \mathbf{0}$), our results state that the recovery is exact. In 1D this is well known, see [9, 10] and the review in Section 3. In 2D and higher, this is new: as explained in Section 4, this result cannot be obtained by a straightforward generalization of the techniques in [9, 10].

2.3 Tightness

In this section we argue that our results in Theorem 2 are nearly tight. In 1D, we are interested in answers to the following two natural questions:

(i) Can the assumption $\mathcal{C} = \mathcal{R}_1^+(3.74r, r)$ be substituted with $\mathcal{C} = \mathcal{R}_1^+(d, r)$ with $d < 3.74r$ without changing the bound (19)?

(ii) Can the exponent $2r$ in (19) be made smaller?

2.3.1 Tightness of the length of the interval

To answer (i), we have already argued in Section 2.1 that even in the noiseless case it is not possible to recover many of the signals $\mathbf{x} \in \mathcal{R}_1^+(d, r)$ with $d < 2r$. Hence, $d = 3.74r$ is within a factor 1.87 of the optimum. This factor comes from the key result from [7] explained above, which concerns the existence of low-frequency polynomials interpolating complex scalars of unit magnitude separated by $1.87\lambda_c$. Any improvement in this technology would yield a corresponding improvement here, see Section 4.1.3 for additional details.

2.3.2 Tightness of the exponent

To answer question (ii) above, we need the concept of modulus of continuity (MC).

Definition 2 (Modulus of continuity). Let $\|\cdot\|$ be a norm, $\mathbf{Q}$ a linear operator, and $\mathcal{C}$ a class of signals.[3] The MC is defined as

$$\mathrm{MC}[\mathcal{C}, \mathbf{Q}] \triangleq \sup_{\mathbf{x}_1, \mathbf{x}_2 \in \mathcal{C}} \frac{\|\mathbf{x}_1 - \mathbf{x}_2\|}{\|\mathbf{Q}(\mathbf{x}_1 - \mathbf{x}_2)\|}.$$

We also introduce the simple notion of noise amplification.

Definition 3 (Noise amplification factor). Let $\|\cdot\|$ be a norm, $\mathbf{B}$ a linear operator, and $\mathcal{C}$ a signal class. Suppose an algorithm A produces an estimator $\hat{\mathbf{x}}(\mathbf{s})$ from the model $\mathbf{s} = \mathbf{Bx} + \mathbf{z}$ obeying the uniform stability guarantee

$$\|\hat{\mathbf{x}} - \mathbf{x}\| \leq \mathrm{NAF}[A, \mathcal{C}, \mathbf{B}] \cdot \delta$$

for all $\mathbf{x} \in \mathcal{C}$ and all $\mathbf{z}$ with $\|\mathbf{z}\| \leq \delta$. Then we say that the NAF of A is (at most) $\mathrm{NAF}[A, \mathcal{C}, \mathbf{B}]$.

---

[3]For example, $\mathcal{C}$ may be a class of sparse signals, a class of Rayleigh regular signals, and so on.

The MC is related to the NAF via the following simple facts.

1. If the NAF of an algorithm A is at most $\mathrm{NAF}[A, \mathcal{C}, \mathbf{Q}]$, then

$$\mathrm{NAF}[A, \mathcal{C}, \mathbf{Q}] \geq \mathrm{MC}[\mathcal{C}, \mathbf{Q}].$$

2. Consider the exhaustive search (ES) algorithm (in general intractable) for super-resolving signals in $\mathcal{C}$:

$$\text{find} \quad \hat{\mathbf{x}} \in \mathcal{C} \quad \text{s.t.} \quad \|\mathbf{s} - \mathbf{Q}\hat{\mathbf{x}}\| \leq \delta \tag{ES}$$

with δ chosen so that $\|\mathbf{z}\| \leq \delta$. The NAF of this algorithm satisfies

$$\mathrm{NAF}[\mathrm{ES}, \mathcal{C}, \mathbf{Q}] \leq 2\mathrm{MC}[\mathcal{C}, \mathbf{Q}].$$

We now provide a lower bound on the MC showing that if the noise is arbitrary, no algorithm can have a NAF smaller than $C\mathrm{SRF}^{2r-1}$. Therefore, the exponent $2r$ in (18) is nearly optimal.

Theorem 3. *Take* $\mathbf{Q} = \mathbf{Q}_{\mathrm{tri,1D}}$. *Set r and d to be arbitrary numbers and $\mathcal{C} = \mathcal{R}_1^+(d, r)$ so that by taking $d = \infty$ we would have at most r spikes. Then there exist signals $\mathbf{x} = [x_0 \cdots x_{N-1}]^{\mathsf{T}}, \tilde{\mathbf{x}} = [\tilde{x}_0 \cdots \tilde{x}_{N-1}]^{\mathsf{T}} \in \mathcal{C}$ s.t.*

$$\|\mathbf{x} - \tilde{\mathbf{x}}\|_1 = 1$$

and when $N, n \to \infty$, $N/n \to \mathrm{SRF}$

$$\|\mathbf{Q}(\mathbf{x} - \tilde{\mathbf{x}})\|_1 \to \chi(r, \mathrm{SRF})\mathrm{SRF}^{2r-1}.$$

For $\mathrm{SRF} \to \infty$,

$$\chi(r, \mathrm{SRF}) \to C_L(r)$$

where $C_L(r)$ depends on r only and is given explicitly in (45). Consequently, letting $\|\cdot\|$ be $\|\cdot\|_1$ in Definition 2,

$$\mathrm{MC}[\mathcal{C}, \mathbf{Q}] \geq C_L(r)\mathrm{SRF}^{2r-1} \tag{20}$$

when N, n and $\mathrm{SRF} = N/n$ are large.

The proof, given in Appendix A, relies on an explicit construction of nonnegative signals $\mathbf{x}$ and $\tilde{\mathbf{x}}$ with disjoint supports and such that the spikes in $\mathbf{x} - \tilde{\mathbf{x}}$ cancel out as much as possible after low-pass filtering.

Comparing Theorems 3 and 2, we see that the exponent of SRF in the right-hand side (RHS) of (18) is within one unit of the best possible. It is important to point out that the convex optimization algorithm in (CVX) knows nothing at all about the regularity of the signal class $\mathcal{C}$. Yet, it is adaptive in the sense that it has nearly optimal stability guarantee whatever the (usually unknown) value of r.

Theorem 3 tells us that the MC increases exponentially with r. For example, for a practically interesting case where $\mathrm{SRF} = 8$, it is not difficult to estimate from (20) and the numerical value of the constant that super-resolution could only be possible if $r \leq 5$. For $r > 5$, the modulus of continuity is greater than 10^5, setting unrealistic constraints on noise levels in practical applications. This is even an optimistic estimate and, in reality, it is nearly impossible to separate more than three sources packed in a Nyquist interval.

It is not known whether the exponent in the lower bound (20) is sharp. In the very special case where the signal contains exactly one spike, it is not difficult to see that a simple matched-filter

11

will have a bounded ratio NAF/SRF, matching the exponent in the RHS of (20). This can be used in the setting where the spikes are guaranteed to be so far apart, that the overlap between their images in the output space can be neglected; this only happens when the distance between neighboring spikes far exceeds $\lambda_c/2$ and all the spikes have roughly the same magnitude. In general, in the interesting case where the images of neighboring spikes can overlap in the output space, it is not clear how one could close the small gap between (20) and (18). In fact, it is possible that the exponent in (20) can be made larger. As we shall see, to construct adversarial signals $\mathbf{x}, \tilde{\mathbf{x}}$ in the proof of Theorem 3, we only use signals that contain exactly r spikes each. However, the signals in $\mathcal{R}_1^+(d, r)$ can have more than r spikes, of course, which could allow one to construct pairs $\mathbf{x}, \tilde{\mathbf{x}}$ that give a larger bound than that in the RHS of (20). Please also see the recent preprint [11], where the question of calculating the exact exponent for signals with a total of r spikes is addressed.

3 Literature review and innovations

3.1 Prior art

Algebraic methods. Prony's method [12] is an algebraic approach for solving the 1D super-resolution problem from noiseless data when the number of sources is known a priori. The data $\mathbf{s}$ is used to form a trigonometric polynomial, whose roots coincide with the spike locations. The polynomial is then factored, thus revealing those locations, and the amplitudes estimated by solving a system of linear equations. In the noiseless case, Prony's method recovers $\mathbf{x}$ perfectly provided that $\|\mathbf{x}\|_0 < n/2$. No further Rayleigh regularity assumption on the signal support is needed. With noise, however, the performance of Prony's method degrades sharply. The difficulty comes from the fact that the roots of a trigonometric polynomial constructed by an algebraic method are completely unstable and can shift dramatically even with small changes in the data.

Many noise-aware versions of Prony's method are used frequently in engineering applications, for example in radar (see [13, Chapter 6]). The most popular methods are MUSIC and its numerous variations [14–19], matrix-pencil [20], and ESPRIT [21, 22]. For more details on algebraic methods we refer the reader to the excellent book [13, Chapter 4]. However, the stability of noise-aware algebraic methods is not theoretically well-understood. Asymptotic results (at high SNR) on the stability of MUSIC in the presence of Gaussian noise are derived in [23, 24]. More recently, some steps towards analyzing MUSIC and matrix-pencil in a non-asymptotic regime have been taken in [25] and in [26], respectively. Nevertheless, to the best of our knowledge, no strong theoretical stability guarantees like those in Theorems 1 and 2 are available for algebraic methods. Hence, the search for super-resolution methods that perform well empirically and have sharp theoretical stability guarantees is an important open problem.

Algebraic methods have been generalized to the multi-dimensional case. Surprisingly, the generalizations are not straightforward and many methods ([27], [28], [13, Sec. 4.9.7]) have very restrictive sparsity constraints: namely, at most n spikes when we recall, that in 2D the total number of observations is n^2. In [29], the number of spikes can be as large as $n^2/4$ in the noiseless case, as one would expect from dimension-counting considerations.

Fundamental limits. In the pioneering work [6], Donoho studied limits of performance for the 1D super-resolution problem. His main findings can be summarized as follows. Put $\|\cdot\| = \|\cdot\|_2$ in the definition of NAF and $\mathbf{Q} = \mathbf{Q}_{\text{flat,1D}}$.

- Let $\mathcal{C} = \mathcal{R}_1(4r, r)$, then the NAF of the exhaustive search algorithm (ES) obeys

$$\mathrm{NAF}[\mathrm{ES}, \mathcal{C}, \mathbf{Q}] \leq C(r)\mathrm{SRF}^{2r+1}, \tag{21}$$

  where $C(r)$ is a positive constant that might depend on r but not on N or n.

- Take an arbitrary pair (r, d) and set $\mathcal{C} = \mathcal{R}_1(d, r)$. Then

$$\mathrm{MC}[\mathcal{C}, \mathbf{Q}] \geq C(r)\mathrm{SRF}^{2r-1},$$

  where $C(r)$ is a positive constant that might depend on r but not on N or n.

To the best of our knowledge, the analysis in [6] has not been generalized to the multi-dimensional case. Unfortunately, The algorithm (ES) is not feasible because $\mathcal{C}$ is not convex, and [6] does not propose any tractable algorithm that would have NAF bounded above by the RHS of (21). In this respect, the key question posed by Donoho is whether a feasible algorithm that achieves stability in (21) exists.

Other works [30–32] study the stability of the super-resolution problem in the presence of noise, but likewise do not provide a tractable algorithm to perform recovery. Work in [33–35] analyzes the detection and separation of two closely-spaced spikes, but does not generalize to the case when there are more than two spikes in the signal.

Super-resolution under minimum separation constraint. Progress towards resolving the question posed in [6] in the general situation where $\mathbf{x} \in \mathbb{C}^N$—in this paper we consider the case $\mathbb{R}_+^N$ only—has recently been made [7, 8]. Put $\|\cdot\| = \|\cdot\|_1$ in the definition of the NAF, select the PSF with a flat spectrum, $\mathbf{Q} = \mathbf{Q}_{\mathrm{flat},1\mathrm{D}}$, and consider $\mathcal{C} = \mathcal{R}_1(4, 1)$. It was shown that the NAF of the ℓ_1-minimization algorithm

$$\min_{\hat{\mathbf{x}}} \|\hat{\mathbf{x}}\|_1 \quad \text{s.t.} \quad \|\mathbf{s} - \mathbf{Q}\hat{\mathbf{x}}\|_1 \leq \delta \tag{L1}$$

with δ chosen so that $\|\mathbf{z}\| \leq \delta$ is at most

$$\mathrm{NAF}[\mathrm{L1}, \mathcal{C}, \mathbf{Q}] \leq C \cdot \mathrm{SRF}^2, \tag{22}$$

where C is a positive numerical constant. The condition $\mathbf{x} \in \mathcal{C} = \mathcal{R}_1(4, 1)$ is restrictive because it means that the signal $\mathbf{x}$ cannot contain spikes that are at a distance less than $2\lambda_c$. [For real-valued signals $\mathbf{x} \in \mathbb{R}^N$, a minimum separation of $1.87\lambda_c$ suffices.] This is a limitation for many applications including single-molecule microscopy, as it is usually understood that the goal of super-resolution is to distinguish spikes that are (significantly) closer than the Rayleigh diffraction limit, i.e. at a fraction of λ_c apart. Unfortunately, if there are spikes at a distance lower than this value, ℓ_1 minimization does not, in general, return the correct solution even if there is no noise. Results in [7,8] also cover the multi-dimensional case under a minimum separation constraint. On a similar line of research, see [36] and [37] for related results on the denoising of line spectra and on the recovery of sparse signals from a random subset of their low-pass Fourier coefficients. The accuracy of support detection under the minimum separation constraint is analyzed in [38,39].

Super-resolution of noiseless nonnegative signals. The case of 1D nonnegative signal, $\mathbf{x} \in \mathbb{R}_+^N$, was analyzed in [9], see also [10] for a shorter exposition of the same idea. Adapting to our setting, the result in [9] can be summarized as follows: put $\|\cdot\| = \|\cdot\|_1$ in the definition of NAF and

$\mathbf{Q} = \mathbf{Q}_{\text{flat,1D}}$. Let $\mathcal{C}$ be the class of all signals with $\|\mathbf{x}\|_0 < n/2$. Then the NAF^{cvx} of the convex feasibility program

$$\text{find } \hat{\mathbf{x}} \geq \mathbf{0} \quad \text{s.t.} \quad \|\mathbf{s} - \mathbf{Q}\hat{\mathbf{x}}\|_2 \leq \delta \tag{F}$$

with δ chosen so that $\|\mathbf{z}\|_2 \leq \delta$, is a finite positive constant. The exact dependence of NAF^{cvx} on N and n is not specified in [9]. As we will see, further examination of the proof from [9] leads to a bound of the form

$$\text{NAF}^{\text{cvx}}[\mathcal{C}, \mathbf{Q}] \leq (CN)^{2\|\mathbf{x}\|_0}, \tag{23}$$

where C is a numerical constant. First, this does not depend on the Rayleigh regularity of $\mathbf{x}$ but on the sparsity. Second, this does not depend on the SRF but on the grid size. By comparing to (21) and (22) we see that the bound (23) is weak. Indeed, consider the interesting case $N, n \to \infty$ with $N/n = \text{SRF}$ kept constant. In this case the bounds in (21) and (22) remain finite, whereas the RHS of (23) converges to $+\infty$ very quickly. The bound in (23) does not depend on the frequency cut-off f_c or equivalently the number n of pieces of information we are given. Whether the frequency cut-off is 10 or 10^6 the bound remains the same! This cannot capture the right behavior.

3.2 Innovations

The novelty of our results can be summarized as follows.

- As compared to algebraic methods, Theorems 1 and 2 show that efficient algorithms can recover the signal in a provably stable fashion. As we discussed earlier, strong worst-case stability guarantees are not available for algebraic methods. The flipside is that our results crucially rely on non-negativity of the signal; algebraic methods do not need this assumption.

- As compared to [6], our recovery algorithm is a simple linear program (LP) and, hence, is tractable whereas the exhaustive search method of [6] is intractable and cannot be used in practice. The difference between stability exponents in (18) and in (21) stem from the fact that [6] works with the ℓ_2 norm while we work with ℓ_1. (The stability bounds for the exhaustive search algorithm in [6] do not assume the signal to be nonnegative.)

- As compared to [7], our results do not rely on the restrictive minimum-separation assumption. Having said this, the results in [7] hold for the general case of complex amplitudes, and our proofs borrow heavily from the tools developed in that work.

- As compared to work in [9], our stability estimates are far stronger, for they depend on the super-resolution factor, and not on the spacing on the fine grid. Further, if one tries to use the proof technique used in [9] to generalize the noiseless results in [9, 10] to the 2D case, one would need to assume that our image has at most $n/2$ spikes: this is too restrictive. In sharp contrast, we see from Theorems 1 and 2 that if the signal support is Rayleigh regular, we may have a number of sources on the order of n^2, i.e. on the order of the number of measurements.

4 Proofs

4.1 Proof of Theorem 1 in the 1D case

The proof of the theorem is based on the following lemma.

Lemma 1. *Assume that the assumptions of Theorem 1 are satisfied. Set*

$$\mathbf{h} = [h_0 \cdots h_{N-1}]^{\mathsf{T}} = \hat{\mathbf{x}} - \mathbf{x}$$

and

$$\mathcal{T} = \{l/N : h_l < 0\}, \tag{24}$$

and suppose there exists $\mathbf{q} = [q_0 \cdots q_{N-1}]^{\mathsf{T}} \in \mathbb{R}^N$ *and* $0 < \rho < 1$ *such that* $\mathbf{Q}\mathbf{q} = \mathbf{q}$, $\|\mathbf{q}\|_\infty \leq 1$, *and*

$$\begin{cases} q_l = 0, & l/N \in \mathcal{T} \\ q_l > 2\rho, & otherwise. \end{cases} \tag{25}$$

Then

$$\|\hat{\mathbf{x}} - \mathbf{x}\|_1 \leq \frac{2(1-\rho)}{\rho} \cdot \|\mathbf{z}\|_1. \tag{26}$$

Proof. Set $\tilde{\mathbf{q}} = [\tilde{q}_0 \cdots \tilde{q}_{N-1}]^{\mathsf{T}} = \mathbf{q} - \rho$ and note that $\|\tilde{\mathbf{q}}\|_\infty \leq 1 - \rho$ since $\rho \leq 1/2$. On the one hand,

$$\begin{aligned} |\langle \tilde{\mathbf{q}}, \mathbf{h} \rangle| = |\langle \mathbf{Q}\tilde{\mathbf{q}}, \mathbf{h} \rangle| &= |\langle \tilde{\mathbf{q}}, \mathbf{Q}\mathbf{h} \rangle| \\ &\leq \|\tilde{\mathbf{q}}\|_\infty \|\mathbf{Q}\mathbf{h}\|_1 \\ &\leq (1-\rho)\|\mathbf{Q}\mathbf{x} - \mathbf{s} + \mathbf{s} - \mathbf{Q}\hat{\mathbf{x}}\|_1 \\ &\leq (1-\rho)(\|\mathbf{Q}\mathbf{x} - \mathbf{s}\|_1 + \|\mathbf{s} - \mathbf{Q}\hat{\mathbf{x}}\|_1) \\ &\leq 2(1-\rho)\|\mathbf{Q}\mathbf{x} - \mathbf{s}\|_1 \\ &= 2(1-\rho) \cdot \|\mathbf{z}\|_1. \end{aligned} \tag{27}$$

On the other hand, using $\text{sign}(\tilde{q}_l) = \text{sign}(h_l)$ for all l gives

$$|\langle \tilde{\mathbf{q}}, \mathbf{h} \rangle| = \left| \sum_{l=0}^{N-1} \tilde{q}_l h_l \right| = \sum_{l=0}^{N-1} \tilde{q}_l h_l = \sum_{l=0}^{N-1} |\tilde{q}_l||h_l| \geq \rho \|\mathbf{h}\|_1, \tag{28}$$

Combining (27) and (28) yields the conclusion. $\qquad\square$

4.1.1 Localization of trigonometric polynomials

Lemma 1 shows that in order to obtain a tight bound we need to construct a (dual) vector $\mathbf{q}$ obeying $\|\mathbf{q}\|_\infty \leq 1$ and (25) with ρ as large as possible. First, observe that since $\mathbf{x}, \hat{\mathbf{x}} \geq \mathbf{0}$ it follows that $\mathcal{T}$ in (24) satisfies $|\mathcal{T}| \leq \|\mathbf{x}\|_0 < n/2$. The idea is to construct a real-valued trigonometric polynomial of largest frequency f_c (recall $n = 2f_c + 1$)

$$q(t) = \sum_{k=-f_c}^{f_c} \hat{q}_k e^{-\mathrm{i}2\pi kt} \in \mathbb{R} \quad \text{for all} \quad t, \tag{29}$$

obeying $\|q\|_\infty \leq 1$,

$$\begin{cases} q(t) = 0, & \text{for all} \quad t \in \mathcal{T}, \\ q(t) > 0, & \text{for all} \quad t \notin \mathcal{T}, \end{cases}$$

and set $\mathbf{q} = \{q(l/N) : l \in [0 : N-1]\}$. Observe that such a $\mathbf{q}$ would obey the conditions of Lemma 1 with $\rho = \frac{1}{2} \arg \min_{l/N \notin \mathcal{T}} \{q(l/N)\}$.

A classical approach to constructing such a polynomial $q(t)$ is

$$q(t) = \prod_{t_0 \in \mathcal{T}} \frac{1}{2} \left[\cos(2\pi(t - t_0) + \pi) + 1 \right]. \tag{30}$$

This approach, used in [9, 10], works whenever $|\mathcal{T}| < n/2$ since the degree of $q(t)$ is then at most f_c. The problem is that $q(t)$ in (30) grows extremely slowly around its zeros, making ρ very small, which then translates into highly suboptimal stability estimates. To demonstrate this, assume that $\mathcal{T} = \{0\}$, i.e., $|\mathcal{T}| = 1$. Then (see Figure 3)

$$q(t) = \frac{1}{2} \left[\cos(2\pi t + \pi) + 1 \right] \tag{31}$$

so that

$$q(1/N) \leq \frac{\pi^2}{N^2}$$

and $\rho \leq \frac{\pi^2}{2N^2}$. Plugging this into (26) we get an estimate no better than

$$\|\hat{\mathbf{x}} - \mathbf{x}\|_1 \leq \frac{2}{\pi^2} N^2 \cdot \|\mathbf{z}\|_1. \tag{32}$$

This is weak. In the case when $\mathbf{x}$ has one spike, the separation condition $\mathcal{T} \in \mathcal{R}_1(3.74, 1)$ of [7] is trivially satisfied. The results in [7] guarantee that ℓ_1 minimization achieves

$$\|\hat{\mathbf{x}} - \mathbf{x}\|_1 \leq C \cdot \frac{N^2}{n^2} \cdot \|\mathbf{z}\|_1 = C \cdot \mathrm{SRF}^2 \cdot \|\mathbf{z}\|_1,$$

where C is a numerical constant. The reason why [7] provides stability guarantees far stronger than (32) is that the trigonometric polynomial $q(t)$ constructed in [7] grows around its zeros much faster than $q(t)$ in (31). We review the behavior of $q(t)$ constructed in [7] in Lemma 2 below and illustrate the difference between this polynomial and that in (31). Based on the results of [7], we then present a novel construction for $q(t)$ that does not rely on the minimal separation condition $\mathcal{T} \in \mathcal{R}_1(3.74, 1)$ needed in [7] and works for all signals with Rayleigh regular support of the type $\mathcal{T} \in \mathcal{R}_1(3.74r, r)$. At the same time, the new polynomial $q(t)$ grows rapidly around its zeros, which allows us to derive strong stability guarantees.

4.1.2 Main building block: $q(t)$ under separation

The following lemma is an immediate consequence of [7, Lm. 2.5] adapted to the case of real-valued signals as explained in [7, Sec. 2.5].

Lemma 2. *Assume $\mathcal{T} \in \mathcal{R}_1(3.74, 1; N, n)$. As before, $f_c = (n - 1)/2$, $\lambda_c = 1/f_c$ and suppose $f_c \geq 128$. Then there exists a real-valued polynomial $q(t) = \sum_{k=-f_c}^{f_c} \hat{q}_k e^{-\mathrm{i}2\pi kt}$ with $\|q\|_\infty \leq 1$ such that*

$$\begin{cases} q(t) = 0, & \text{for all } t \in \mathcal{T}, \\ q(t) \geq \phi(t), & \text{for all } t, \end{cases}$$

where (see Figure 3)

$$\phi(t) = \begin{cases} c_1 f_c^2 (t_0 - t)^2, & \text{for all } t \text{ s.t. } \exists t_0 \in \mathcal{T} \text{ with } |t - t_0| \leq c_2 \lambda_c \\ c_1 f_c^2 (c_2 \lambda_c)^2 = c_1 c_2^2, & \text{otherwise}, \end{cases} \tag{33}$$
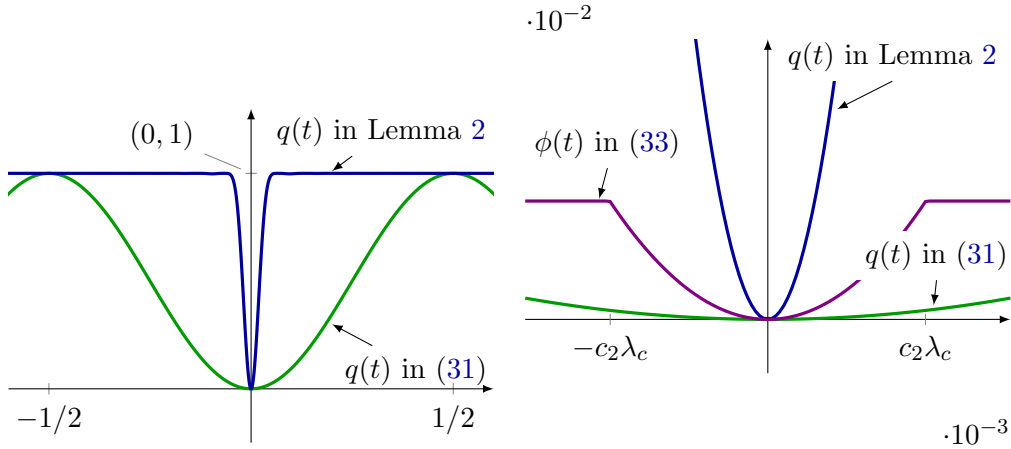
and $c_1 = 0.029$, $c_2 = 0.17$.

16

Figure 3: Comparison of trigonometric polynomials at two different scales: the polynomial from [7] (see Lemma 2) bounces off zero much faster than that used in [9, 10].

The significance of this lemma is that the growth of $q(t)$ around its zeros is nearly optimal. Indeed, suppose we wish to construct a real nonnegative polynomial with highest frequency f_c of the form (29) of magnitude at most one, and which grows around its zeroes as fast as possible. How fast could it possibly grow? Since $q(t)$ is a superposition of harmonic functions, it cannot outpace a pure harmonic—normalized to take on values in $[0, 1]$—at the highest available frequency. Hence, we cannot hope for growth faster than

$$\frac{1}{2}\left[\cos(2\pi f_c(t - t_0) + \pi) + 1\right] \approx \pi^2 f_c^2(t - t_0)^2 \quad \text{for small } t. \tag{34}$$

Comparing (34) to (33), we see that Lemma 2 provides a construction that is optimal up to at most a constant factor.

We now show how to extend the construction in Lemma 2 to the case where the elements of $\mathcal{T}$ are not necessarily well-separated, but $\mathcal{T}$ is Rayleigh regular. Together with Lemma 1, this will prove Theorem 1. The proof below is illustrated on Figure 4, which the reader is encouraged to consult while following the argument.
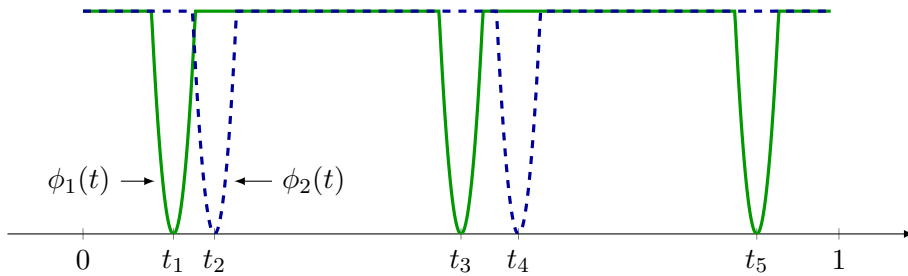

Figure 4: Illustration of the proof of Theorem 1 for $r = 2$; $\mathcal{T}_1 = \{t_1, t_2, t_3\}$; $\mathcal{T}_2 = \{t_2, t_4\}$. The trigonometric polynomials $q_1(t)$, $q_2(t)$ satisfy $q_1(t) = 0$ for all $t \in \mathcal{T}_1$ and $q_2(t) = 0$ for all $t \in \mathcal{T}_2$; they are not displayed. The lower bounds $\phi_1(t)$ and $\phi_2(t)$ defined in (35) are depicted.

17

4.1.3 Construction of $q(t)$ without separation

Take $\mathbf{x} \in \mathcal{R}_1^+(3.74r, r)$ with a support of cardinality S. Define $\mathbf{h}$ and $\mathcal{T} = \{t_k\}_{k=1}^S$ with $t_1 < t_2 < \ldots < t_S$ as in Lemma 1. Since h_l can only take on negative values on $\text{supp}(\mathbf{x})$, then $\mathcal{T} \in \mathcal{R}_1(3.74r, r)$. Consider the partition $\mathcal{T} = \cup_{i=1}^r \mathcal{T}_i$, where $\mathcal{T}_i = \{t_{rk+i}\}_{k=0}^{S/r-1}$. Since $\mathcal{T} \in \mathcal{R}_1(3.74r, r)$, $\mathcal{T}_i \in \mathcal{R}_1(3.74r, 1)$ and by rescaling,

$$\mathcal{R}_1(3.74r, 1; N, n) = \mathcal{R}_1(3.74, 1; N, \tilde{n}),$$

where $\tilde{n} = (n-1)/r + 1$. Set[4] $\tilde{f}_c = (\tilde{n}-1)/2 = (n-1)/(2r) = f_c/r$ and $\tilde{\lambda}_c = 1/\tilde{f}_c = r/f_c$. By Lemma 2, there are real-valued polynomials $q_i(t; N, \tilde{n}) = \sum_{k=-\tilde{f}_c}^{\tilde{f}_c} \hat{q}_{ik} e^{-\mathrm{i}2\pi kt}$ with $\|q_i\|_\infty \leq 1$ and

$$\begin{cases} q_i(t) = 0, & \text{for all } t \in \mathcal{T}_i, \\ q_i(t) \geq \phi_i(t), & \text{for all } t, \end{cases}$$

where (see Figure 4)

$$\phi_i(t) = \begin{cases} c_1 \tilde{f}_c^{\,2}(t_0 - t)^2, & \text{for all } t \text{ s.t. } \exists t_0 \in \mathcal{T}_i \text{ with } |t - t_0| \leq c_2 \tilde{\lambda}_c, \\ c_1 \tilde{f}_c^{\,2}(c_2 \tilde{\lambda}_c)^2 = c_1 c_2^2, & \text{otherwise.} \end{cases} \tag{35}$$

The trigonometric polynomial q is obtained by taking the product of the q_i's:

$$q(t) = \prod_{i=1}^r q_i(t; N, \tilde{n}).$$

By construction, $q(t)$ is band-limited, i.e., $q(t) = \sum_{k=-f_c}^{f_c} \hat{q}_k e^{-\mathrm{i}2\pi kt}$, $\|q\|_\infty \leq 1$, and

$$\begin{cases} q(t_0) = 0, & \text{for all } t_0 \in \mathcal{T}, \\ q(t) \geq \prod_{i=1}^r \phi_i(t), & \text{for all } t. \end{cases} \tag{36}$$

Next we further lower-bound $\prod_{i=1}^r \phi_i(t)$. Fix t and let $\mathcal{N} = \{t_1, \ldots, t_{\hat{r}}\} = \{\hat{t} \in \mathcal{T} : |t - \hat{t}| \leq c_2 \tilde{\lambda}_c\}$. Since $\mathcal{T} \in \mathcal{R}_1(3.74r, r)$, it follows that $\hat{r} \leq r$. Let t_0 be the closest element of $\mathcal{N}$ to t so that $(t_0 - t)^2 \leq (t_i - t)^2$ for all $i = 1, \ldots, \hat{r}$. By the definition of $\mathcal{N}$, $c_1 \tilde{f}_c^{\,2}(t_i - t)^2 \leq c_1 c_2^2$. Using (35) and these inequalities we may write

$$\prod_{i=1}^r \phi_i(t) \geq (c_1 c_2^2)^{r-\hat{r}} c_1^{\hat{r}} \tilde{f}_c^{2\hat{r}} \prod_{i=1}^{\hat{r}} (t_i - t)^2$$

$$\geq \begin{cases} c_1^r \tilde{f}_c^{\,2r}(t_0 - t)^{2r}, & \text{for all } t \text{ s.t. } \hat{r} > 0 \\ (c_1 c_2^2)^r, & \text{otherwise.} \end{cases} \tag{37}$$

The assumption $\text{SRF} \geq 3/r$ implies $\text{SRF} = N/n > 1/(2rc_2) \approx 2.94/r$, which is equivalent to $1/N < c_2 r2/n$ so that $1/N < c_2 \tilde{\lambda}_c$. Therefore, from (36) and (37), it follows that

$$\rho = \frac{1}{2} \arg \min_{l/N \notin \mathcal{T}} \{q(l/N)\} \geq c_1^r \frac{1}{2} \tilde{f}_c^{\,2r} \frac{1}{N^{2r}} = c_1^r \frac{1}{2r^{2r}} f_c^{2r} \frac{1}{N^{2r}} = c_1^r \frac{1}{2(2r)^{2r}} \left(\frac{n-1}{N} \right)^{2r}. \tag{38}$$

---

[4] Strictly speaking, this requires f_c/r to be an integer. If f_c/r is not an integer, we can substitute f_c with $r\lfloor f_c/r \rfloor$ and repeat the argument for the new f_c. Since $f_c \geq 128r$ by assumption, this transformation will result in less than a 1% change meaning that $\mathcal{R}_1(3.74r, r)$ would need to change into $\mathcal{R}_1(3.77r, r)$. To keep things simple, we ignored this detail throughout the paper and implicitly assumed that f_c/r is an integer.

Plugging this into (26) gives

$$\|\hat{\mathbf{x}} - \mathbf{x}\|_1 \leq \underbrace{4c_3^r r^{2r}}_{C_1(r)} \left(\frac{N}{n-1}\right)^{2r} \cdot \|\mathbf{z}\|_1, \tag{39}$$

where $c_3 = 4/c_1 = 67.79$. This completes the proof. $\qquad\square$

Remark (Possible Improvement). The constant 3.74 in $\mathbf{x} \in \mathcal{R}_1^+(3.74r, r)$ comes from the fact that our construction is built on top of Lemma 2 borrowed from [7, Sec. 2.5]. If the constant 3.74 in Lemma 2 is reduced, all our results automatically improve without any modification. Carlos Fernandez-Granda privately shared with us [40] that it is possible to substitute 3.74 by 2.52 in Lemma 2.

Remark (Extension). Consider a signal consisting of spike clusters as shown in Figure 5, and violating the separation constraint. Suppose that within each cluster, the spikes have the same sign. Then our proof technique can be used to show that if the clusters are sufficiently separated, the signal can be recovered stably by convex programming. We omit the details.

Figure 5: Signal with clustered spikes that have the same sign within a cluster but different signs across clusters.

4.2 Proof of Theorem 2 in the 1D case

Our strategy is to reduce the problem to that in which we have a flat spectrum. Choose $1/2 \leq \alpha < 1$ (a parameter we can optimize) so that αf_c is an integer, and define the filter

$$\hat{r}_k \triangleq \begin{cases} \frac{f_c+1}{f_c+1-|k|}, & k = -\alpha f_c, \ldots, \alpha f_c, \\ (f_c+1)\left(a|k|+b\right), & |k| = \alpha f_c + 1, \ldots, f_c, \\ 0, & \text{otherwise.} \end{cases}$$

with

$$a \triangleq -\frac{1}{f_c(1-\alpha)+1}\frac{1}{f_c(1-\alpha)} \quad \text{and} \quad b \triangleq \frac{1}{f_c(1-\alpha)+1}\frac{1}{1-\alpha}.$$

Set $\hat{\mathbf{R}} \triangleq \text{diag}(\hat{\mathbf{r}})$ with $\hat{\mathbf{r}} \triangleq [\hat{r}_{-N/2+1} \cdots \hat{r}_{N/2}]^\mathsf{T}$ and let $\mathbf{R} \triangleq \mathbf{F}^\mathsf{H}\hat{\mathbf{R}}\mathbf{F}$. The point is that

$$\mathbf{T} \triangleq \mathbf{RQ} = \mathbf{F}^\mathsf{H}\hat{\mathbf{R}}\mathbf{F}\mathbf{F}^\mathsf{H}\hat{\mathbf{Q}}\mathbf{F} = \mathbf{F}^\mathsf{H}\hat{\mathbf{R}}\hat{\mathbf{Q}}\mathbf{F} = \mathbf{F}^\mathsf{H}\hat{\mathbf{T}}\mathbf{F}$$

has a spectrum $\hat{\mathbf{T}} \triangleq \text{diag}([\hat{t}_{-N/2+1} \cdots \hat{t}_{N/2}]^\mathsf{T})$ given by

$$\hat{t}_k \triangleq \begin{cases} 1, & k = -\alpha f_c, \ldots, \alpha f_c, \\ \left(f_c + 1 - |k|\right)\left(a|k|+b\right), & |k| = \alpha f_c + 1, \ldots, f_c, \\ 0, & \text{otherwise.} \end{cases}$$

Figure 6: In (a), $\mathcal{T} \in \mathcal{R}_2(9.52, 2)$ has eight elements and can be decomposed as $\mathcal{T} = \mathcal{T}_1 \cup \mathcal{T}_2$ with $\mathcal{T}_1, \mathcal{T}_2 \in \mathcal{R}_2(9.52, 1)$. The points in $\mathcal{T}_1$ are in blue and those in $\mathcal{T}_2$ are in green. In (b), $\mathcal{T}$ has eight points belonging to a line parallel to a coordinate axis; this is a worst-case scenario.

Note that the spectrum of $\mathbf{T}$ is flat in the region $-\alpha f_c \leq k \leq \alpha f_c$. Next, construct $\mathbf{q}$ as in Section 4.1 with f_c replaced by αf_c. Because $\mathbf{q}$ is band-limited to αf_c, $\mathbf{Tq} = \mathbf{q}$. On the one hand,

$$
\begin{aligned}
|\langle \mathbf{q}, \mathbf{h} \rangle| = |\langle \mathbf{Tq}, \mathbf{h} \rangle| &= |\langle \mathbf{q}, \mathbf{Th} \rangle| \\
&\leq \|\mathbf{q}\|_\infty \|\mathbf{Th}\|_1 \\
&\leq (1 - \rho)\|\mathbf{RQx} - \mathbf{Rs} + \mathbf{Rs} - \mathbf{RQ\hat{x}}\|_1 \\
&\leq (1 - \rho)\|\mathbf{R}\|_{1,op} \left(\|\mathbf{Qx} - \mathbf{s}\|_1 + \|\mathbf{s} - \mathbf{Q\hat{x}}\|_1 \right) \\
&\leq 2(1 - \rho)\|\mathbf{R}\|_{1,op}\|\mathbf{Qx} - \mathbf{s}\|_1 \\
&\leq 2(1 - \rho)C(\alpha) \cdot \|\mathbf{z}\|_1.
\end{aligned}
$$

The last step follows from Appendix C, where we show that for all N and all SRF,

$$
\|\mathbf{R}\|_{1,op} \leq C(\alpha) \triangleq 2\alpha + \frac{2}{1 - \alpha} + \frac{1.11}{2(1 - \alpha)^2}. \tag{40}
$$

Note that $C(\alpha)$ is finite as long as $\alpha < 1$. For $\alpha = 1/2$, $C(\alpha) = 7.22$. For $\alpha = 0.75$, $C(\alpha) = 18.38$. On the other hand, $|\langle \mathbf{q}, \mathbf{h} \rangle| \geq \rho\|\mathbf{h}\|_1$ as before, where ρ is given in (38) with the substitution $n - 1 = 2f_c \to 2\alpha f_c$. In conclusion,

$$
C = C_1(r, \alpha) = C_1(r)C(\alpha)\left(\frac{1}{\alpha}\right)^{2r}. \tag{41}
$$

4.3 Remarks on Theorems 1 and 2 in 2D

The proof of the 2D version of Theorem 1 closely mimics that in the 1D case. Since $\mathbf{x} \in \mathcal{R}_2^+(4.76r, r)$, we can work with a partition $\mathcal{T} = \cup_{1 \leq i \leq r} \mathcal{T}_i$ with $\mathcal{T}_i \in \mathcal{R}_2(4.76r, 1)$. This is illustrated in Figure 6 for $r = 2$. The proof follows the same steps as in Section 4.1. The dual trigonometric polynomial is constructed as a product of r polynomials. The i-th term in the product has zeros on $\mathcal{T}_i$ and is constructed using Lemma 4 given in Appendix D for completeness; this lemma is a 2D version of Lemma 2, and its proof can be found in [7, Prop. C.1], [8, Sec. D.1]. The proof of Theorem 2 in the 2D case follows the steps outlined in Section 4.2 with slight modifications, which are omitted.

To the best of our knowledge, Theorem 1 is the first result, in the noisy and in the noiseless setting, showing that the 2D super-resolution problem can be solved via convex optimization when

20

the signal is nonnegative, without assuming a separation condition. It is instructive to discuss this point in details as the discussion reveals interesting insights about the super-resolution problem in higher dimensions.

Suppose one would like to obtain a noiseless result for nonnegative signals similar to that in [9, 10]. Following Section 4.1.1 one could take a 2D version of the polynomial in (31),

$$\frac{1}{4} \left[\cos(2\pi t_1 + \pi) + 1 \right] \left[\cos(2\pi t_2 + \pi) + 1 \right] \tag{42}$$

and then form a product of such terms to build a low-frequency polynomial $q(t_1, t_2)$ as done in (30). What is the largest number of terms the product in (30) could contain in the 2D setting? Since each term of the form (42) costs two units in the frequency domain in each variable, to be able to guarantee that $q(t_1, t_2)$ has frequency no larger than f_c in both variables, one can have no more that $n/2$ terms of the form (42). Because each term in the product is zero only at one point of the support, this technique would not guarantee recovery of signals with more than $n/2$ spikes. This is discouraging since we have have n^2 observations. It is easy to see that $\|\mathbf{x}\|_0 < n/2$ is a tight bound in the worst case: think about the situation where the support is located along a line parallel to a coordinate axis as in Figure 6(b). In this case, even though we have n^2 observations, the problem is essentially one-dimensional with n observations and no more that $n/2$ spikes can possibly be resolved.

However, what happens in the typical situation where the spikes are Rayleigh regularly spread over the domain as in Figure 6(a)? In this case, we construct the trigonometric polynomial, which is a product of r terms as in the 2D version of (37). Each term in the product has frequencies at most n/r and vanishes at $\sim n^2/r^2$ points of the support simultaneously. For example, in Figure 6(a) all the elements in $\mathcal{T}_1$ are roots of the first term and all those in $\mathcal{T}_2$ are roots of the second. Hence, as Theorem 1 shows, the number of spikes can be as large as

$$\frac{(n-1)^2}{4.76^2 r^2} r \approx \frac{n^2}{4.76^2 r};$$

i.e. for a fixed value of r, $\|\mathbf{x}\|_0$ may grow linearly with the number of observations. This is a much stronger result compared to what would be achievable via the method from [9, 10].

5   Numerical results

This section introduces a numerical simulation to illustrate the effectiveness of our method in super-resolution microscopy. Set $f_c = 19$, SRF $= 10$, so that $N = 390$ and consider the 2D model with $\mathbf{Q} = \mathbf{Q}_{\text{tri,2D}}$.

- The image $\mathbf{x}$ of dimensions 390×390 dimensional is shown in Figure 7b. This image contains five different regions with different source densities: (i) the top-left quarter is a signal from $\mathcal{R}_2(4.28, 1)$; (ii) the top-right quarter is from $\mathcal{R}_2(2.14, 1)$; (iii) the lower-left quarter is from $\mathcal{R}_2(4.28, 2)$; (iv) the lower-right quarter towards the center is from $\mathcal{R}_2(2.24, 2)$; (v) and the lower-right quarter towards the corner contains three closely co-located spikes. All spikes were chosen to have equal magnitude set to $10,000$. To be clear, we are performing one large experiment in which different regions of $\mathbf{x}$ exhibit different spike densities; we run the reconstruction algorithm only once. (Overall, the signal would need to belong to $\mathcal{R}_2(\cdot, 3)$ since it contains three spikes in a Nyquist cell.)

- The observations, displayed in Figure 7a, are generated according to the model $\mathbf{s} = \text{Pois}(\mathbf{Qx})$.

We solve the LP (CVX) by smoothing the objective into $h_\mu(\mathbf{s} - \mathbf{Q}\hat{\mathbf{x}})$, where h_μ is the Huber function defined as $h_\mu(\mathbf{y}) = \sum_i h_\mu(y_i)$, where

$$h_\mu(t) = \begin{cases} \frac{1}{2}t^2/\mu, & |t| \le \mu, \\ |t| - \mu/2, & |t| > \mu. \end{cases}$$

This is a smooth approximation to the ℓ_1 norm, and is tight when μ is small [41]. To make sure our approximation is really tight, we set $\mu_0 = 0.1 \cdot \|\sqrt{\mathbf{s}}\|_1/N^2 \approx 0.1 \cdot \|\mathbf{s} - \mathbf{Q}\mathbf{x}\|_1/N^2$. We then solve the smooth problem using Lan/Lu/Monteiro's primal-dual first order method [42] with a solver written in the framework provided by TFOCS [43]. There are two implementation details worth mentioning. First, we start the algorithm from an initial guess obtained by the frequently used continuation method. That is, we solve a series of three smoother problems (so that convergence is faster) with $\mu \in \{10^3\mu_0, 10^2\mu_0, 10\mu_0\}$, each time taking the solution to the previous problem as an initial guess. To solve these intermediate problems, the stopping criterion is a relative ℓ_2 error between two consecutive iterations below 10^{-5} or a number of iterations reaching 1000, whichever occurs first. Second, for the value of $\mu = \mu_0$, we perform $15,000$ iterations of the Lan/Lu/Monteiro's method to obtain a precise solution. This is an overkill but at the same time, this guarantees that we are solving (CVX). For information, the total computational cost is about 40,000 2D fast Fourier transforms (FFTs) of size 390×390.

The signal estimate is displayed in Figure 7c. In Figure 7d we zoomed-in to six interesting domains of the images in Figure 7a–Figure 7c, which are marked by white boxes in Figure 7a. In each series of three images in Figure 7d we present the data, the original signal, and the estimate produced by (CVX).

As we can see, in the regions (i), (ii), (iii) the algorithm performs very well, resolving even the closely located pairs of spikes in region (iii) (please see the zoomed-in vignettes). In region (iv) the algorithm fails in many places, and region (v) is very poorly resolved. The reason for the poor resolution in regions (iv) and (v) is that in (iv), the average density of spikes is too high. In region (v) there are too many spikes located within one Nyquist cell.

6 Conclusion

When a signal is positive and Rayleigh regular, then linear programming solves the super-resolution problem with near-optimal worst-case performance. Although the results presented in this paper assume that the signal is supported on a discrete grid, extensions to the continuum can be found in the companion paper [5].

A widely open research problem concerns the super-resolution of complex-valued signals. In 1D, [6] shows that if the signal belongs to $\mathcal{R}_1(4r, r)$, then stable super-resolution is possible via exhaustive search. If the signal belongs to $\mathcal{R}_1(4, 1)$, [7] proves that stable super-resolution can be achieved via ℓ_1-minimization. Is there a computationally feasible algorithm that achieves stable super-resolution for signals in $\mathcal{R}_1(4r, r)$ with $r > 1$? If no such algorithm is found, is it possible to show that this problem is in some sense fundamentally difficult from a computational viewpoint?
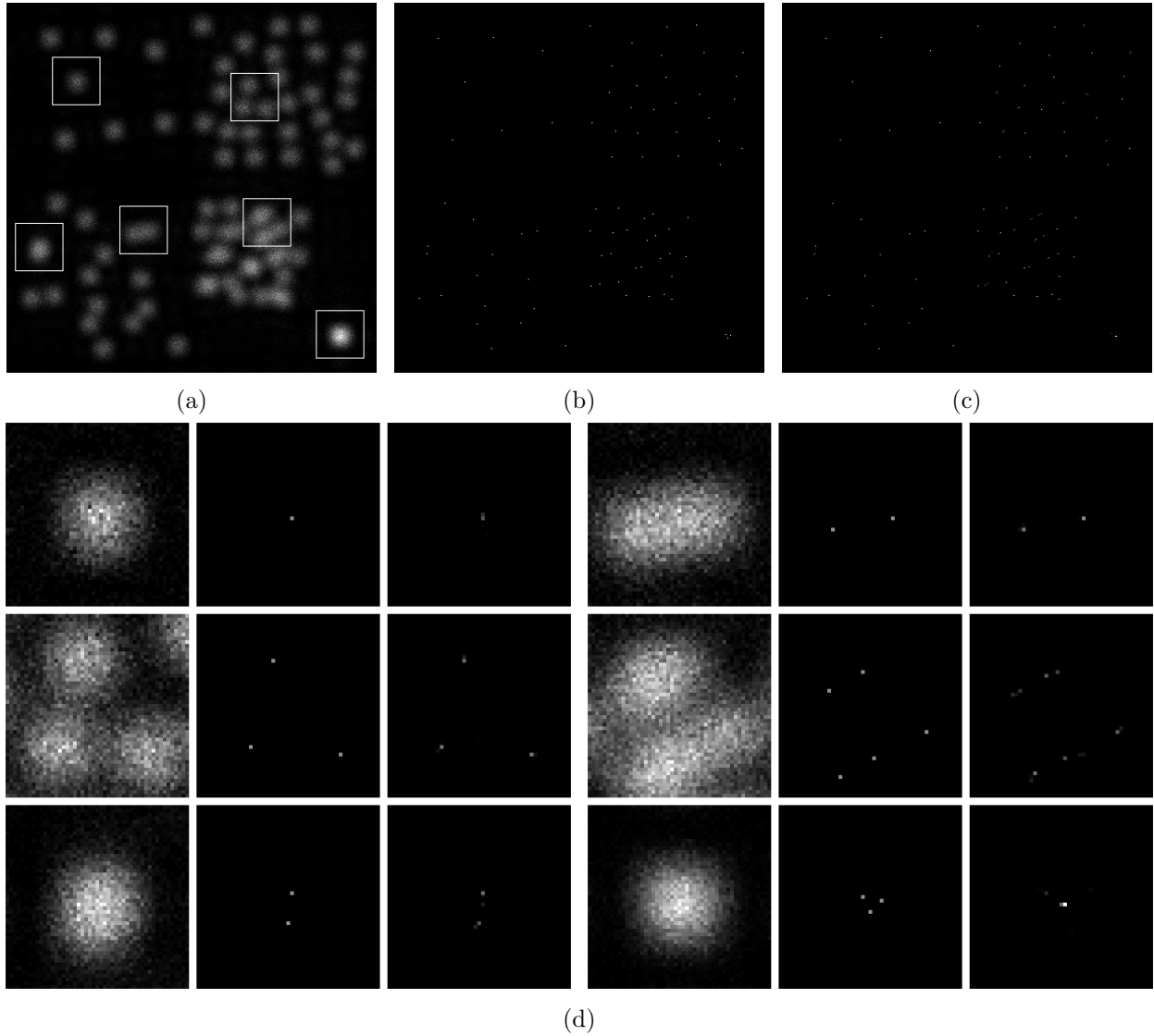
Acknowledgments

Figure 7: (a) Observed data $\mathrm{Pois}\,(\mathbf{Q}_{\mathrm{tri,2D}}\mathbf{x})$; (b) true signal $\mathbf{x}$; (c) estimate produced by (CVX); (d) six zoomed-in vignettes corresponding to the boxes in (a); the rows-of-three in (d) show the observed data, the true signal and the estimate in this order.

A   Proof of Theorem 3

The proof uses the idea of [9, Th. 4] with an important difference: there, the authors provide a lower bound on a modulus of continuity defined as $\sup_{\mathbf{x}_1,\mathbf{x}_2\in\mathcal{C}} \|\mathbf{x}_1 - \mathbf{x}_2\|_1/\|\mathbf{Q}_{\text{flat,1D}}(\mathbf{x}_1 - \mathbf{x}_2)\|_2$. In our case, we are interested in a lower bound on $\text{MC}[\mathcal{C},\mathbf{Q}] \triangleq \sup_{\mathbf{x}_1,\mathbf{x}_2\in\mathcal{C}} \|\mathbf{x}_1 - \mathbf{x}_2\|_1/\|\mathbf{Q}(\mathbf{x}_1 - \mathbf{x}_2)\|_1$.

Put $\mathbf{h} = [h_0\cdots h_{N-1}]^{\mathsf{T}} = \mathbf{x} - \tilde{\mathbf{x}}$ and $\mathbf{s} = [s_0\cdots s_{N-1}]^{\mathsf{T}} = \mathbf{Qh}$. Then a standard calculation shows that s_m can be written as

$$s_m = \sum_{l=0}^{N-1} g_{\text{low}}\left(\frac{m-l}{N}\right) h_l, \tag{43}$$

where

$$g_{\text{low}}(t) = \frac{1}{(1+f_c)N}\left(\frac{\sin((1+f_c)\pi t)}{\sin(\pi t)}\right)^2$$

is the Fejér kernel. The idea is to construct $\mathbf{h}$ with at most $2r$ nonzero elements in such a way that for each m, the terms in the sum (43) cancel each other out as much as possible. One way to do this in a systematic way is to set

$$x_k = \begin{cases} \frac{1}{2^{2r-1}}\binom{2r-1}{k}, & k \in \{0,2,\ldots,2(r-1)\} \\ 0, & \text{otherwise.} \end{cases}, \quad \tilde{x}_k = x_{k-1}$$

(with the periodic convention). Obviously, $\|\mathbf{x}\|_0 = \|\tilde{\mathbf{x}}\|_0 = r$ and setting $\omega = 2r-1$ for convenience,

$$\|\mathbf{h}\|_1 = \|\mathbf{x} - \tilde{\mathbf{x}}\|_1 = \frac{1}{2^\omega}\sum_{l=0}^{\omega}\binom{\omega}{l} = 1.$$

With this,

$$s_m = \sum_{l=0}^{\omega} \underbrace{(-1)^l\frac{1}{2^\omega}\binom{\omega}{l}}_{h_l} g_{\text{low}}\left(\frac{m-\omega}{N} + \frac{\omega-l}{N}\right) = \frac{1}{2^\omega}\Delta_{1/N}^{\omega}[g_{\text{low}}]\left(\frac{m-\omega}{N}\right),$$

where

$$\Delta_\delta^\omega[g_{\text{low}}](t) = \sum_{l=0}^{\omega}(-1)^l\binom{\omega}{l}g_{\text{low}}(t+(\omega-l)\delta)$$

is the finite-difference operator of order ω applied to the kernel $g_{\text{low}}(\cdot)$. For large N and large SRF, $\Delta_{1/N}^{\omega}[g_{\text{low}}](t) \approx \frac{1}{N^\omega}\frac{d^\omega g_{\text{low}}}{dt^\omega}(t)$, a crucial fact allowing us to obtain closed-form estimates on $\|\mathbf{s}\|_1$. Formally, write s_m as a Fourier series

$$s_m = \frac{1}{N}\sum_{k=-f_c}^{f_c} e^{\mathrm{i}2\pi mk/N} q\left(\frac{k}{f_c+1}\right) p_\omega\left(\frac{k}{N}\right),$$

where

$$q(f) = \begin{cases} 1-|f|, & f \in [-1,1], \\ 0, & \text{otherwise,} \end{cases}$$

and

$$p_\omega(f) = \sum_{l=0}^{\omega} e^{-\mathrm{i}2\pi lf} h_l.$$

24

Now let

$$t_m = \int_{-(f_c+1)/N}^{(f_c+1)/N} e^{i2\pi mf} q\left(f\frac{N}{f_c+1}\right) p_\omega(f) df. \tag{44}$$

It is not difficult to see that for all N

$$\sum_{m=-N/2+1}^{N/2} |t_m - s_m| \leq \sum_{|m|\geq N/2} |t_m|$$

and, therefore, since the series $\sum_{m=-\infty}^{\infty} |t_m|$ converges,

$$\|\mathbf{s}\|_1 = \sum_{m=0}^{N-1} |s_m| = \sum_{m=-N/2+1}^{N/2} |s_m| \to \sum_{m=-\infty}^{\infty} |t_m|$$

when $N, n \to \infty$ with $N/n = \mathrm{SRF}$ fixed. Using the fact that $q(f) = 0$ for $|f| > 1/2$ and changing variables in the integral in (44) we can write

$$t_m = \int_{-(f_c+1)/N}^{(f_c+1)/N} e^{i2\pi mf} q\left(\frac{fN}{f_c+1}\right) p_\omega(f) df$$

$$= \frac{f_c+1}{N} \int_{-1}^{1} e^{i2\pi(m(f_c+1)/N)f} q(f)\, p_\omega\left(\frac{f(f_c+1)}{N}\right) df.$$

We conclude that as $N, n \to \infty$ with $N/n = \mathrm{SRF}$ fixed,

$$\|\mathbf{s}\|_1 \to \left(\frac{1}{\mathrm{SRF}}\right)^\omega \frac{1}{\chi(r, \mathrm{SRF})}$$

where,

$$\frac{1}{\chi(r,\eta)} \triangleq \frac{1}{2^\omega}\frac{1}{2\eta} \sum_{m=-\infty}^{\infty} \left| \int_{-1}^{1} e^{i2\pi(m/(2\eta))f} q(f)\, (2\eta)^{2r-1} p_{2r-1}(f/(2\eta)) df \right|.$$

Since the finite difference operator converges to the derivative operator as $\delta \to 0$:

$$\frac{1}{\delta^\omega} \Delta_\delta^\omega [g_{\mathrm{low}}](\cdot) \to \frac{d^\omega(\cdot)}{dt^\omega}, \quad \delta \to 0,$$

it follows that for every fixed f,

$$\eta^\omega p_\omega(f/\eta) \to \frac{1}{2^\omega}(i2\pi f)^\omega, \quad \eta \to \infty.$$

Therefore, when $\mathrm{SRF} \to \infty$,

$$\chi(r, \mathrm{SRF}) \to C_L(r)$$

where

$$C_L(r) \triangleq 2^{2r-1} \left(\pi^{2r-1} \int_{-\infty}^{\infty} \left| \int_{-1}^{1} e^{i2\pi tf} q(f) f^{2r-1} df \right| dt \right)^{-1}. \tag{45}$$

Direct numerical computation reveals

$$C_L(r) \geq \begin{cases} 1.66, & r = 1 \\ 1.44, & r = 2 \\ 0.92, & r = 3 \\ 0.48, & r = 4 \\ 0.24, & r = 5. \end{cases}$$

B   Coherent Optics

When the illumination is perfectly coherent, the time-varying phasor amplitudes across the object plane differ only by complex constants so that we can write

$$\Phi(\mathbf{w}, t) = \Phi(\mathbf{w})\frac{\Phi(0, t)}{\sqrt{\langle|\Phi(0, t)|^2\rangle}}.$$

Plugging this into (5) we obtain

$$\tilde{s}_{\mathrm{coh}}(\mathbf{v}) \propto \left|\int h(\mathbf{v} - \mathbf{w})\Phi(\mathbf{w})d\mathbf{w}\right|^2. \tag{46}$$

We see that in a coherent imaging system, the directly observable received intensity, $\tilde{s}_{\mathrm{coh}}(\mathbf{v})$, is a nonlinear (quadratic) function (46) of the signal $\Phi(\mathbf{w})$.

C   Proof of 40

By definition, $\mathbf{R} = [\mathbf{r}_0 \cdots \mathbf{r}_{N-1}]$ is a circulant matrix, and, hence, $\|\mathbf{R}\|_{1,op} = \|\mathbf{r}_0\|_1$. Further, by properties of circulant matrices,

$$\hat{\mathbf{r}} = \sqrt{N}\mathbf{F}\mathbf{r}_0$$

or, equivalently,

$$\mathbf{r}_0 = \frac{1}{\sqrt{N}}\mathbf{F}^{\mathsf{H}}\hat{\mathbf{r}}$$

so that

$$\|\mathbf{R}\|_{1,op} = \frac{1}{\sqrt{N}}\|\mathbf{F}^{\mathsf{H}}\hat{\mathbf{r}}\|_1.$$

We use the following lemma.

Lemma 3. *Assume $\hat{u}_l$ is a discrete periodic signal with period N. For each l, let*

$$\hat{v}_l = \hat{u}_l - \hat{u}_{l-1}, \tag{47}$$
$$\hat{w}_l = \hat{v}_l - \hat{v}_{l-1} \tag{48}$$

be the first and second differences of $\hat{u}_l$. Let u_k, v_k, w_k be N-periodic sequences of inverse DFT coefficients of $\hat{u}_l, \hat{v}_l, \hat{w}_l$, respectively. For example,

$$u_k = \frac{1}{\sqrt{N}}\sum_{l=-N/2+1}^{N/2} \hat{u}_l e^{2\pi i l k/N}.$$

Assume that

$$\sum_{k=-N/2+1}^{N/2} |\hat{w}_k| \leq A.$$

Then for all $k \neq 0 \mod N$,

$$|u_k| \leq \frac{1}{\sqrt{N}}\frac{A}{2 - 2\cos(2\pi k/N)} \quad \textit{for all} \quad k \neq 0 \mod N.$$

Proof. By the theorem about the DFT of first differences [44, p. 223],

$$w_k = \left(1 - e^{2\pi ik/N}\right)^2 u_k$$

and, consequently,

$$u_k = \frac{1}{\left(1 - e^{2\pi ik/N}\right)^2} w_k \quad \text{for all} \quad k \neq 0, \pm N, \pm 2N, \dots. \tag{49}$$

Next, observe that

$$|w_k| \leq \frac{1}{\sqrt{N}} \sum_{l=-N/2+1}^{N/2} |\hat{w}_l| \leq \frac{A}{\sqrt{N}}. \tag{50}$$

Substituting (50) into (49) and using that $|1 - \exp(2\pi ik/N)|^2 = 2 - 2\cos(2\pi k/N)$ concludes the proof. $\square$

Set $\hat{u}_l = \hat{r}_l$, continued periodically with period N, and define $\hat{v}_l, \hat{w}_l$ as in (47) and (48). Observe the following facts:

$$
\begin{aligned}
\hat{v}_k &= 0, & k &\in [-N/2 + 1 : -\beta f_c], \\
\hat{v}_k &= (f_c + 1)|a|, & k &\in [-f_c + 1 : -\alpha f_c], \\
\hat{v}_{-\alpha f_c + 1} &= -\frac{f_c + 1}{((1-\alpha)f_c + 1)((1-\alpha)f_c + 2)} = -\hat{v}_{\alpha f_c}, & & \\
\hat{v}_k &= -(f_c + 1)|a|, & k &\in [\alpha f_c + 1 : f_c], \\
\hat{v}_k &= 0, & k &\in [f_c + 1 : N/2]
\end{aligned}
$$

and note that $\hat{v}_k$ is monotonically increasing on the intervals $[-N/2 + 1 : -\alpha f_c]$, $[-\alpha f_c + 1 : \alpha f_c]$ and $[\alpha f_c + 1 : N/2]$. From this it immediately follows that

$$\sum_{k=-N/2+1}^{-\alpha f_c} |\hat{w}_k| = \sum_{k=-f_c+1}^{-\alpha f_c} |\hat{w}_k| = \hat{v}_{-\alpha f_c} - \hat{v}_{-f_c} = (1 + f_c)|a|,$$

$$|\hat{w}_{-\alpha f_c + 1}| = \frac{f_c + 1}{((1-\alpha)f_c + 1)((1-\alpha)f_c + 2)} + (f_c + 1)|a| = |\hat{w}_{\alpha f_c + 1}|,$$

$$\sum_{k=-\alpha f_c+2}^{\alpha f_c} |\hat{w}_k| = \hat{v}_{\alpha f_c} - \hat{v}_{-\alpha f_c + 1} = 2\frac{f_c + 1}{((1-\alpha)f_c + 1)((1-\alpha)f_c + 2)},$$

$$\sum_{k=\alpha f_c+2}^{N/2} |\hat{w}_k| = \hat{v}_{f_c + 1} - \hat{v}_{\alpha f_c + 1} = (f_c + 1)|a|$$

so that

$$\sum_{k=-N/2+1}^{N/2} |\hat{w}_k| = 4\frac{f_c + 1}{((1-\alpha)f_c + 1)((1-\alpha)f_c + 2)} + 4(f_c + 1)|a| \leq A$$

where

$$A \triangleq \frac{1}{(f_c + 1)} \underbrace{\frac{4}{(1-\alpha)^2}}_{D} + \frac{2}{f_c} \underbrace{\frac{2}{(1-\alpha)^2}}_{E}.$$

Furthermore, a direct calculation reveals that

$$|u_k| \leq \frac{1}{\sqrt{N}} \sum_{l=-N/2+1}^{N/2} |\hat{u}_l|$$

$$= \frac{1}{\sqrt{N}} \left[1 + 2 \left(\sum_{l=1}^{\alpha f_c} |\hat{u}_l| + \sum_{l=\alpha f_c+1}^{f_c} |\hat{u}_l| \right) \right]$$

$$\leq \frac{1}{\sqrt{N}} \left[1 + 2 \left(\frac{\alpha f_c}{2} \left(1 + \frac{f_c+1}{(1-\alpha)f_c+1} \right) + \frac{f_c+1}{2((1-\alpha)f_c+2)} - \frac{f_c+1}{((1-\alpha)f_c+1)((1-\alpha)f_c+2)} \right) \right]$$

$$\leq \frac{f_c}{2\sqrt{N}} \underbrace{\left(2\alpha + \frac{2}{1-\alpha} \right)}_{B}.$$

Finally, (40) follows from

$$\frac{1}{\sqrt{N}} \|\mathbf{F}^{\mathsf{H}} \hat{\mathbf{r}}\|_1 = \frac{1}{\sqrt{N}} \sum_{k=-N/2+1}^{N/2} |u_k|$$

$$\leq \frac{2}{\sqrt{N}} \sum_{k=0}^{N/(f_c+1)} |u_k| + \frac{2}{\sqrt{N}} \sum_{k=N/(f_c+1)+1}^{N/2} |u_k|$$

$$\leq \frac{f_c}{N} \frac{N}{f_c+1} B + \frac{2A}{N} \sum_{k=N/(f_c+1)+1}^{N/2} \frac{1}{2 - 2\cos(k2\pi/N)}$$

$$\leq B + \frac{D}{2\pi^2} + \frac{E}{2\pi^2} \frac{2(f_c+1)}{f_c}$$

$$\leq B + \frac{D}{2\pi^2} + 3\frac{E}{2\pi^2},$$

where we used that

$$\sum_{k=N/(f_c+1)+1}^{N/2} \frac{1}{2 - 2\cos(k2\pi/N)} \leq \int_{N/(f_c+1)}^{N/2} \frac{1}{2 - 2\cos(f2\pi/N)} df$$

$$= \frac{N \cot(\pi/(f_c+1))}{4\pi}$$

$$= \frac{N(f_c+1)}{4\pi} \frac{\cot(\pi/(f_c+1))}{(f_c+1)}$$

and

$$\frac{\cot(\pi/(f_c+1))}{(f_c+1)} \leq \frac{1}{\pi} \quad \text{for all} \quad (f_c+1) \geq 0.$$

D   Basic Lemma in the 2D case

Lemma 4. *Fix N, n and assume $\mathcal{T} \in \mathcal{R}_2(4.76, 1)Nn$. Set $f_c = (n-1)/2, \lambda_c = 1/f_c$ and suppose $f_c \geq 512$. Then there exists a real-valued trigonometric polynomial*

$$q(\mathbf{t}; N, n) = \sum_{k_1=-f_c}^{f_c} \sum_{k_2=-f_c}^{f_c} \hat{q}_{k_1,k_2} e^{-\mathrm{i}2\pi(k_1 t_1 + k_2 t_2)}, \quad \mathbf{t} = [t_1, t_2]^{\mathsf{T}},$$

such that $\|q\|_\infty \leq 1$, *and*

$$\begin{cases} q(\mathbf{t}) = 0, & \text{for all} \quad \mathbf{t} \in \mathcal{T} \\ q(\mathbf{t}) \geq \phi(\mathbf{t}), & \text{for all} \quad \mathbf{t}, \end{cases}$$

where

$$\phi(\mathbf{t}) = \begin{cases} c_1 f_c^2 \|\mathbf{t}_0 - \mathbf{t}\|_2^2, & \text{for all } \mathbf{t} \text{ s.t. } \exists \mathbf{t}_0 \in \mathcal{T} \text{ with } \|\mathbf{t} - \mathbf{t}_0\|_\infty \leq c_2 \lambda_c \\ c_3 \text{ for all } \mathbf{t} \in \left\{ \tilde{\mathbf{t}} : \|\tilde{\mathbf{t}} - \mathbf{t}_0\|_\infty \geq c_2 \lambda_c \text{ for all } \mathbf{t}_0 \in \mathcal{T} \right\}. \end{cases}$$

Above, c_1, c_2, *and* c_3 *are numerical constants.*

References

[1] J. W. Goodman, *Introduction to Fourier Optics.* McGraw-Hill, 1988.

[2] E. Betzig, G. H. Patterson, R. Sougrat, O. W. Lindwasser, S. Olenych, J. S. Bonifacino, M. W. Davidson, J. Lippincott-Schwartz, and H. F. Hess, "Imaging intracellular fluorescent proteins at nanometer resolution," *Science*, vol. 313, pp. 1642–1645, Sept. 2006.

[3] R. M. Dickson, A. B. Cubitt, R. Y. Tsien, and W. Moerner, "On/off blinking and switching behaviour of single molecules of green fluorescent protein," *Nature*, vol. 388, pp. 355–358, July 1997.

[4] T. A. Klar, S. Jakobs, M. Dyba, A. Egner, and S. W. Hell, "Fluorescence microscopy with diffraction resolution barrier broken by stimulated emission," *Proc. Natl. Acad. Sci. USA*, vol. 97, pp. 8206–8210, July 2000.

[5] V. I. Morgenshtern and E. J. Candès, "Super-resolution of positive sources: the continuous setup," 2014. To be submitted, preprint is available upon request.

[6] D. L. Donoho, "Superresolution via sparsity constraints," *SIAM J. Math. Anal.*, vol. 23, pp. 1309–1331, Sept. 1992.

[7] E. J. Candès and C. Fernandez-Granda, "Towards a mathematical theory of super-resolution," *Commun. Pure Appl. Math.*, vol. 67, pp. 906–956, June 2014.

[8] E. J. Candès and C. Fernandez-Granda, "Super-resolution from noisy data," *J. Fourier Anal. Appl.*, vol. 19, pp. 1229–1254, Dec. 2013.

[9] D. L. Donoho, I. M. Johnstone, J. C. Hoch, and A. S. Stern, "Maximum entropy and the nearly black object," *J. Roy. Statist. Soc. Ser. B*, vol. 54, pp. 41–81, June 1992.

[10] J.-J. Fuchs, "Sparsity and uniqueness for some specific under-determined linear systems," in *Proc. IEEE Int. Conf. Acoust., Speech, Signal Process. (ICASSP)*, vol. 5, pp. v/729–v/732, 2005.

[11] L. Demanet and N. Nguyen, "The recoverability limit for superresolution via sparsity," Dec. 2014, arXiv:1502.01385.

[12] R. Prony, "Essai expérimental et analytique," *J. de l'Ecole Polytechnique (Paris)*, vol. 1, no. 2, pp. 24–76, 1795.

[13] P. Stoica and R. Moses, *Spectral Analysis of Signals*. Prentice Hall, 2005.

[14] A. Barabell, "Improving the resolution performance of eigenstructure-based direction-finding algorithms," in *Proc. IEEE Int. Conf. Acoust., Speech, Signal Process. (ICASSP)*, vol. 8, pp. 336–339, 1983.

[15] G. Bienvenu, "Influence of the spatial coherence of the background noise on high resolution passive methods," in *Proc. IEEE Int. Conf. Acoust., Speech, Signal Process. (ICASSP)*, vol. 4, pp. 306–309, 1979.

[16] R. O. Schmidt, "Multiple emitter location and signal parameter estimation," *IEEE Trans. Antennas Propagat.*, vol. AP-34, pp. 276–280, Mar. 1986.

[17] V. F. Pisarenko, "The retrieval of harmonics from a covariance function," *Geophysical J. Int.*, vol. 33, no. 3, pp. 347–366, 1973.

[18] D. W. Tufts and R. Kumaresan, "Estimation of frequencies of multiple sinusoids: making linear prediction perform like maximum likelihood," *Proc. IEEE*, vol. 70, pp. 975–989, Sept. 1982.

[19] J. A. Cadzow, "Signal enhancement—A composite property mapping algorithm," *IEEE Trans. Acoust., Speech, Signal Process.*, vol. 36, pp. 49–62, Jan. 1988.

[20] Y. Hua and T. K. Sarkar, "Matrix pencil method for estimating parameters of exponentially damped/undamped sinusoids in noise," *IEEE Trans. Acoust., Speech, Signal Process.*, vol. 38, pp. 814–824, May 1990.

[21] A. Paulraj, R. Roy, and T. Kailath, "A subspace rotation approach to signal parameter estimation," *Proc. IEEE*, vol. 74, pp. 1044–1046, July 1986.

[22] R. Roy and T. Kailath, "ESPRIT – estimation of signal parameters via rotational invariance techniques," *IEEE Trans. Acoust., Speech, Signal Process.*, vol. 37, pp. 984–995, July 1989.

[23] H. Clergeot, S. Tressens, and A. Ouamri, "Performance of high resolution frequencies estimation methods compared to the Cramer-Rao bounds," *IEEE Trans. Acoust., Speech, Signal Process.*, vol. 37, pp. 1703–1720, Nov. 1989.

[24] P. Stoica and T. Söderström, "Statistical analysis of MUSIC and subspace rotation estimates of sinusoidal frequencies," *IEEE Trans. Signal Process.*, vol. 39, pp. 1836–1847, Aug. 1991.

[25] W. Liao and A. Fannjiang, "MUSIC for single-snapshot spectral estimation: stability and super-resolution," Apr. 2014, arXiv: 1404.1484.

[26] A. Moitra, "The threshold for super-resolution via extremal functions," Aug. 2014, arXiv:1408.1681v2.

[27] M. P. Clark and L. L. Scharf, "Two-dimensional modal analysis based on maximum likelihood," *IEEE Trans. Signal Process.*, vol. 42, pp. 1443–1452, June 1994.

[28] M. Clark, L. Eldén, and P. Stoica, "A computationally efficient implementation of 2-D IQML," in *Proc. Asilomar Conf. Signals, Syst., Comput.*, vol. 2, pp. 1730–1734, Nov. 1997.

[29] T. Jiang, N. D. Sidiropoulos, and J. M. F. ten Berge, "Almost-sure identifiability of multi-dimensional harmonic retrieval," *IEEE Trans. Signal Process.*, vol. 49, pp. 1849–1859, Sept. 2001.

[30] P. Stoica and A. Nehorai, "Statistical analysis of two nonlinear least-squares estimators of sine-wave parameters in the colored-noise case," *Circuits, Syst. and Signal Process.*, vol. 8, no. 1, pp. 3–15, 1989.

[31] P. Stoica, R. L. Moses, B. Friedlander, and T. Söderström, "Maximum likelihood estimation of the parameters of multiple sinusoids from noisy measurements," *IEEE Trans. Acoust., Speech, Signal Process.*, vol. 37, no. 3, pp. 378–392, 1989.

[32] D. Batenkov and Y. Yomdin, "On the accuracy of solving confluent Prony systems," *SIAM J. Appl. Math.*, vol. 73, pp. 134–154, Jan. 2013.

[33] M. Shahram and P. Milanfar, "Imaging below the diffraction limit: a statistical analysis," *IEEE Trans. Image Process.*, vol. 13, pp. 677–689, May 2004.

[34] M. Shahram and P. Milanfar, "On the resolvability of sinusoids with nearby frequencies in the presence of noise," *IEEE Trans. Signal Process.*, vol. 53, pp. 2579–2588, July 2005.

[35] C. W. Helstrom, "The detection and resolution of optical signals," *IEEE Trans. Inf. Theory*, vol. 10, pp. 275–287, Oct. 1964.

[36] G. Tang, B. N. Bhaskar, and B. Recht, "Near minimax line spectral estimation," *IEEE Trans. Inf. Theory*, vol. 61, pp. 499–512, Jan. 2015.

[37] G. Tang, B. N. Bhaskar, P. Shah, and B. Recht, "Compressed sensing off the grid," *IEEE Trans. Inf. Theory*, vol. 59, pp. 7465–7490, Nov. 2013.

[38] C. Fernandez-Granda, "Support detection in super-resolution," in *Proc. Conf. on Sampling Theory and Applicat.*, pp. 145–148, 2013.

[39] J.-M. Azaïs, Y. de Castro, and F. Gamboa, "Spike detection from inaccurate samplings," *Appl. Comp. Harm. Anal.*, vol. 38, pp. 177–195, Mar. 2015.

[40] C. Fernandez-Granda, "Super-resolution of point sources via convex programming," 2015. In preparation.

[41] Y. Nesterov, "Smooth minimization of non-smooth functions," *Math. Program.*, vol. 103, pp. 127–152, May 2005.

[42] G. Lan, Z. Lu, and R. D. C. Monteiro, "Primal-dual first-order methods with o(1/) iteration-complexity for cone programming," *Math. Program.*, vol. 126, pp. 1–29, Jan. 2011.

[43] S. R. Becker, E. J. Candes, and M. C. Grant, "Templates for convex cone problems with applications to sparse signal recovery," *Math. Program. Comput.*, vol. 3, no. 3, pp. 165–218, 2011.

[44] A. W. Oppenheim, A. S. Willsky, and S. Hamid, *Signals and Systems*. Prentice Hall, 2nd ed., 1996.